

Modeling the effects of supercomplex formation and stress response on
Alzheimer's disease progression

Morgan Griffin Shelton

West Point, Virginia

Bachelor of Science,
The College of William & Mary, 2017

A Thesis presented to the Graduate Faculty of The College of William
& Mary in Candidacy for the Degree of
Master of Science

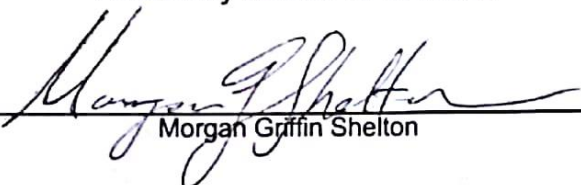
Department of Chemistry

College of William & Mary
May 2019


APPROVAL PAGE

This Thesis is submitted in partial fulfillment of
the requirements for the degree of


Chemistry Master of Science



Morgan Griffin Shelton

Approved by the Committee April 2019


Committee Chair
Professor Randolph Coleman, Chemistry
College of William & Mary


Professor Lisa Landino, Chemistry
College of William & Mary


Professor Nathaniel Kidwell, Chemistry
College of William & Mary


Professor Frank Castora
Eastern Virginia Medical School

ABSTRACT

Alzheimer's disease is a specific form of dementia characterized by the aggregation of Amyloid- β plaques and tau tangles. New research has found that the formation of these aggregates occurs after dysregulation of respiratory activity and the production of radical oxygen species. Proteomic data shows that these changes are also related to unique gene expression patterns. We investigate the impact of these findings on new therapeutic options via metabolic flux analysis of sirtuin stress response pathways and respiratory supercomplex formation. Our results indicate CRISPR Cas-based gene therapy focused on upregulating stable CIII expression, and protective changes in SIRT1 and AMPK expression are potential avenues for therapeutics. This work also highlights the importance of metabolic enzyme activity in maintaining proper respiratory activity.

TABLE OF CONTENTS

Acknowledgements	ii
Dedication	iii
Introduction	1
Methods	13
Results	18
Discussion	28
References	31
Appendix	39

ACKNOWLEDGEMENTS

I want to thank Professor Coleman for his guidance, patience and criticism throughout the investigation as well as Dr. Castora for thoughtful insight and helping me understand the broader scope of this research. Finally I want to thank Jess Crowley, Sonali Shirali and Zhenyu Han for their invaluable assistance in designing and understanding these models. Without them, I could not have completed this project.

This MS is dedicated to my late grandmothers.

Introduction

Alzheimer's disease (AD) is a neurodegenerative disease characterized by the aggregation of neurofibrillary tangles and amyloid plaques (Cadenas & Davies, 2000; Grimm, Friedland, & Eckert, 2016). It is unclear if these aggregates cause cognitive degeneration or if they are a byproduct of other degenerative stimuli (Herrup, 2015). However, it is becoming increasingly apparent that mitochondrial impairment plays a significant role in the onset and progression of AD (Cai, Yan, Li, Quazi, & Zhao, 2012). Current research suggests that the mitochondrial efficiency plays a significant role on when and if a person develops dementia (Grimm et al., 2016; Mancuso, Orsucci, Siciliano, & Murri, 2008). With these new findings, researchers are looking into new ways to understand AD by studying changes in mitochondrial activity. Synthesis of this new research and older findings have produced two new theories about AD onset. The two theories are the Inverse Warburg Hypothesis (IW) and the Mitochondrial Cascade Hypothesis (MC) which explain the relationship between mitochondrial impairment and characteristic plaque buildup.

Both the IW and MC theories were created to explain late onset AD (LOAD; Campion et al., 1999). The IW postulates that, prior to degeneration, there is an unsustainable increase in metabolic demand by neurons to compensate for respiratory inefficiency. Because neurons do not process glucose directly, they rely on astrocytes to process glucose into lactate which is then transferred from the astrocytes to the nearby neurons (Demetrius & Simon, 2013). One dysfunctional neuron's elevated metabolic demand consumes a high concentration of the astrocyte's limited glucose pool. The high consumption leaves nearby, healthy neurons lacking essential metabolites. Eventually the entire neuronal system begins collapsing leading to apoptosis and memory loss (Grimm

et al., 2016). There is no recorded evidence of the initial increase in metabolic demand that the IW theory predicts making it difficult to prove.

The MC hypothesis claims that genetics determine an innate level of respiratory chain efficiency. As people age, respiratory activity slows producing less ATP and more H_2O_2 . During this process, minor impairments in the respiratory chain become more apparent. The subsequently high levels of ROS leave the mitochondria more susceptible to oxidative damage (Mosconi, 2013; Swerdlow, Burns, & Khan, 2010). ROS accumulation leads to activation of transcription factors peroxisome proliferator-activates receptor gamma, coactivator 1 (PGC1 α) and forkhead box O3 (FOXO3) to increase mitochondrial biogenesis or induce autophagic pathways (Brenmoehl & Hoeflich, 2013). Proteomic data showing differences in gene expression support this theory. Compared to control tissue, nuclear encoded mitochondrial subunit expression is suppressed, and cell death related pathways are upregulated.

We have created two models to investigate how changes in respiratory activity explained by these hypotheses influence mitochondrial viability as well as changes in stress signaling. Based on proteomic data, we investigated the impact changes in nuclear encoded subunits play in respiratory efficiency as well as how the related ROS production can influence gene transcription. During this investigation, we hope to better understand how the mitochondria reduces and responds to long term increases in oxidative stress as well as how to leverage these pathways to treat a serious underlying problem in AD affected brain cells.

Respiratory Modeling

Respiration is the process of oxidizing NADH and $FADH_2$ to release electrons which reduce Coenzyme Q (CoQ) before being transferred to cytochrome C (cyt C) and

eventually convert O₂ gas into water. This process is carried out across multiple respiratory complexes (RC), which pump high concentration of protons from the matrix into the intermembrane space (Murphy, 2009). A few decades ago, this was believed to occur across individual complexes embedded in the inner membrane. Today, two different models, fluid and solid state, have been proposed to describe how this transfer takes place. The fluid model which describes the electron transport chain (ETC) as separate complexes within the membrane. Once loaded or unloaded, CoQ and Cyt c diffuse until they reach the next complex in the RC (Letts, Fiedorczuk, & Sazanov, 2016). The solid state model proposes that individual complexes assemble to form a large multimeric complex known as the respirasome to be functional (Lapiente-Brun et al., 2013). In reality, the mitochondria functions with a spectrum of individual complexes, supercomplexes (SCs; functional intermediaries composed of a fraction of the complexes within the respirasome) and the respirasome. The purpose of these structures is unclear. SCs may reduce the diffusion distance of Cyt c and CoQ which may increase RC efficiency (Milenkovic, Blaza, Larsson, & Hirst, 2017). Researchers have found that formation of the respirasome limits ROS production by stabilizing NADH dehydrogenase (CI) structure and covering one oxygen binding site on CI which plays a role in mitochondrial stress signaling (Stroud et al., 2016). SC assembly varies with cell state and type, which indicates SC formation could be physiologically significant and needs further exploration (Lopez-Fabuel et al., 2016).

CI is the largest of the respiratory chain complexes, it oxidizes NADH and transfers the electrons to CoQ. This predominant producer of signaling-linked ROS contains two oxygen binding sites, one of which is protected when CI assembles to form the respirasome and other SCs. The two O₂ binding sites are Flavin mononucleotide (FMN) and N₂ (an iron-sulfur cluster); oxygen binding at either location results in ROS production

(Acín-Pérez, Fernández-Silva, Peleato, Pérez-Martos, & Enriquez, 2008). Reverse electron transport (RET), which inefficiently reduces NAD when the Q pool is highly reduced and results in heightened levels of mitochondrial ROS (Lambert & Brand, 2004). RET occurs when CI, CoQ and later complexes become saturated with electrons. This ROS production seems to be linked to CI in its monomeric form, not as part of a complex with CIII or within the respirasome (Lenaz et al., 2010). Arthur, Morton, Dunham, Keeney, and Bennett (2009) found that the connection may in part be due to a slowed electron flow through CI and higher stability when part of an SC.

If CI is not properly stabilized, increasing concentrations of ROS are produced causing mitochondrial oxidative stress (Cadenas & Davies, 2000; Liu et al., 2010; Ray, Huang, & Tsuji, 2012). This oxidative stress can activate signaling cascades which change gene transcription (Bechtel & Bauer, 2009). Changes in gene transcription can be seen by analyzing the changes in an organism's proteome. Our collaborators with Dr. Castora at Eastern Virginia Medical School have done analyses that show changes in mitochondrial biogenesis with AD. Their analysis of tissues affected by AD indicate that the pathways related to the changes in ROS proliferation, defense, and energy production are altered. Our proposed mitochondrial models (SC assembly and oxidative stress) focus on the effects of oxidative stress on the antioxidant defense system and the induction of stress response signaling cascades. Through careful analysis we propose for effective therapy routes, SIRT1, AMPK and ETC subunit UQCRC1, for *in vitro* AD treatment testing.

Supercomplex assembly model

After individual complexes have formed, complexes CI, Ubiquinone-Cytochrome C Reductase (CIII), and Cytochrome C Oxidase (CIV) begin to associate and form SCs. SCs are stable intermediates between respirasomes (solid state model) and individual complexes (fluid model). The two most prevalent SC compositions are CIVCIII₂ and CICIII₂ (abbreviated CIVCIII and CICIII), the latter being more common (Ramírez-Camacho, Flores-Herrera, & Zazueta, 2019). The work by Maranzana et al. (2013), has implicated SCs in increasing respiratory efficiency and reducing ROS proliferation. SC and

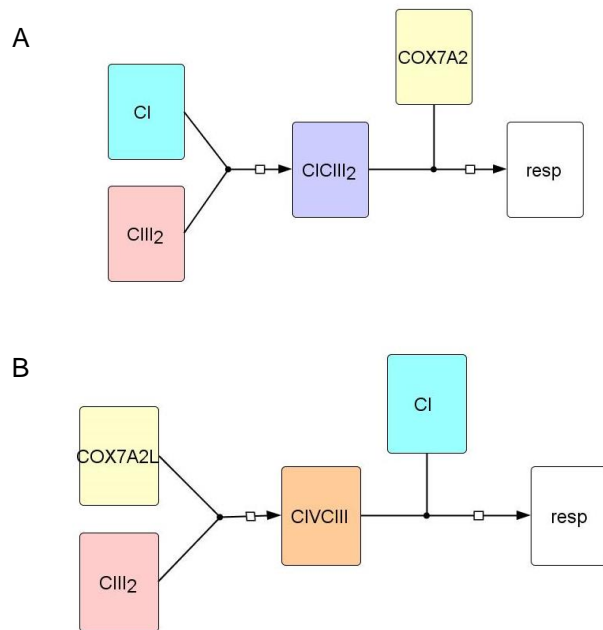


Figure 1A & B:
The two pathways for respirasome formation involve two SC intermediates, CICIII and CIVCIII
A: CICIII forms and assembles with CIV containing the COX7A2 subunit.
B: CIVCIII forms using CIV with the COX7A2L subunit then with CI to form the final respirasome.

respirasome concentrations also vary between cell types. For example, astrocytes have been shown to have lower levels of SC formation, and this increases the basal level of ROS within the mitochondria (Lopez-Fabuel et al., 2016).

Nuclear encoded ETC subunits are used to stabilize complexes as well as assemble SCs and respirasomes. The lesser found SC CIVCIII formation requires the COX7A2L isoform being present in CIV; it results in rapid assembly of the respirasome

(Lobo-Jarne et al., 2018; Figure 1b). COX7A2, the shorter isoform, within CIV leads to CICIII SC intermediate formation before final respirasome formation (Lapuente-Brun et al., 2013; Figure 1a). Within CIII, the expression of subunits, UQCRFS1, UQCRC1 and UQCRB ensure stable association with COX7A2L (Letts et al., 2016). CI association with the CIII dimer (usually forming CICIII₂) reduces ROS formation in the mitochondria making the association highly favorable both *in vivo* and *in vitro* (Greggio et al., 2017). This association utilizes two bonding groups for stabilization including CI subunits NDUFB4

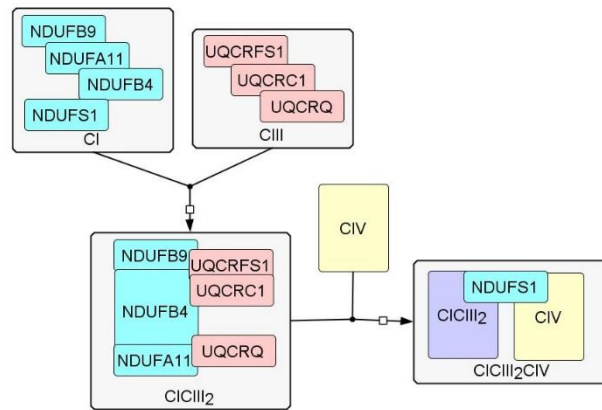


Figure 2: Assembly of SC's. is dependent on the expression of nuclear encoded subunits NDUFB9, NDUFA11, NDUFB4, NDUFS1 in CI and UQCRFS1, UQCRC1, and UQCRQ in CIII

and NDUFB9 which bind to CIII subunits UQCRFS1 and UQCRC1. CICIII also uses NDUFA11 and NDUFB4 to bond with UQCRQ (Letts et al., 2016; Stroud et al., 2016). Absence of one of these subunits does not prevent SC formation, but it does form a less stable association between individual complexes (Acin-Perez & Enriquez, 2014).

An SC with a CICIII₂CIV composition is known as a respirasome, but larger respirasome structures have been reported with up to four CIII and CIV present (Letts et al., 2016). Only 20% of mitochondrial CIV is incorporated into the respirasome compared to 55-65% of CIII and over 85% of CI (Greggio et al., 2017). This near complete

incorporation of CI into SCs supports the hypothesis that all SC formation stabilizes CI and reduces ROS production (Maranzana et al., 2013). Lopez-Fabuel et al. (2016) report that CI subunit NDUFS1 deletion or downregulation has been shown to inhibit respirasome formation. This loss *in vivo* could significantly affect mitochondrial SC composition which in turn can change ROS production and mitochondrial signaling.

Oxidative Stress Modeling

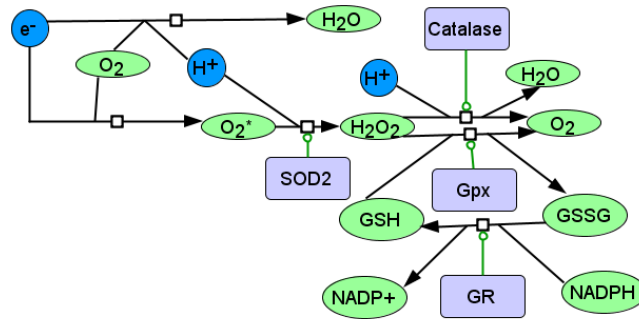


Figure 3: The innate antioxidant system contains three enzymes SOD2, Cat and Gpx which process superoxide through a series of reaction to form inert water and oxygen gas.

Occasionally electrons escape ETC complexes during electron transport and create hydroxyl and superoxide radicals (Figure 3; Murphy, 2009; Sena & Chandel, 2012). Small amounts of ROS production is normal and easily regulated by constitutively expressed antioxidant proteins including superoxide dismutase (SOD2), Glutathione peroxidase (Gpx), Catalase (Cat) (Ighodaro & Akinloye, 2017). These proteins convert ROS into inert water or signaling molecules such as hydrogen peroxide. This is typical mitochondrial activity, but when more ROS is being produced than these antioxidant proteins can handle, oxidative stress signaling activates changes in gene expression to stop ROS accumulation or eliminate dysfunctional mitochondria (Ogura et al., 2018). PGC1 α and FOXO3 are two important transcription factors that mitigate oxidative stress. They lead to the induction of antioxidant and autophagic proteins to include mitophagy

which help eliminate terminally dysfunctional mitochondria and prevent cell apoptosis (Blacker & Duchon, 2016). Mitochondrial biogenesis is also altered by these changes in gene transcription which increase ETC subunit and antioxidant transcription. If these interventions fail, apoptosis is induced to prevent total cell dysfunction and cellular decay (Du & Yan, 2010).

During the process of activating antioxidant systems, autophagy and apoptosis, pathological biomarkers of AD including amyloid aggregates and hyper phosphorylated tau are produced and accumulate, which amplifies these initial changes in gene transcription (Kim, Kim, Rhie, & Yoon, 2015). Based on the mitochondrial cascade hypothesis and the work done by Dr. Castora's research group, we propose that gene therapies focused on reestablishing basal mitochondrial function, increasing ATP (adenosine triphosphate) and decreasing ROS production, we can successfully minimize or halt the accumulation of aggregates.

Pathways

Radical Quenching

The ETC oxidizes NADH and FADH₂ to create the membrane potential for oxidative phosphorylation. During this process, electrons can leak out of the ETC and create ROS (Starkov & Fiskum, 2003). To combat the production of excess ROS, the cell has evolved an antioxidant system involving two lines of defense; initial radical quenching and subsequent alterations in gene transcription (Ighodaro & Akinloye, 2017; Zhang et al., 2018). Sirtuins (SIRT) are a family of proteins predominately found within the cytosol, nucleus, and mitochondria. The two primary SIRTs found in the human brain are SIRT3 and SIRT1 (Brenmoehl & Hoeflich, 2013). SIRT1 and SIRT3 use NAD to modulate the activation of local enzymes (Figure 4). When NADH levels are low and therefore NAD

mononucleotide adenylyltransferase; Figure 4). NAMPT is the rate limiting step in this reaction chain (Ling Liu et al., 2018). Slowing of NAMPT's activity increases the NAM pool (Nikiforov, Dölle, Niere, & Ziegler, 2011).

Radical quenching is performed by the antioxidant enzyme system which includes SOD2, Cat, and Gpx (Ighodaro & Akinloye, 2017). Cat and SOD2 have low levels of activity under normal conditions, but SIRT3 increases their activity as ROS accumulates in the matrix (Chen et al., 2011; Rangarajan et al., 2015). This allows the mitochondria to conserve their energy and only induce energy demanding changes in gene expression under periods of stress. SOD2 converts radical oxygen into peroxide (Sun, Oberley, & Li, 1988). Gpx uses two monomers of glutathione (GSH) to convert peroxide into water creating a glutathione dimer (GSSG) in the process. GSSG is then reduced to GSH by glutathione reductase (GR) so that Gpx can continue processing the peroxide being produced by SOD2 (Carlberg & Mannervik, 1975; Ighodaro & Akinloye, 2017). When there is a high concentration of glutathione dimers, common under oxidative stress conditions, SIRT3 deacetylates IDH2, catalyzing the reduction of glutathione dimers back to their monomeric state. (Yu, Dittenhafer-Reed, & Denu, 2012). If peroxide levels get too high, Cat will begin to convert the excess peroxide into water and oxygen (Bechtel & Bauer, 2009).

Response Pathways

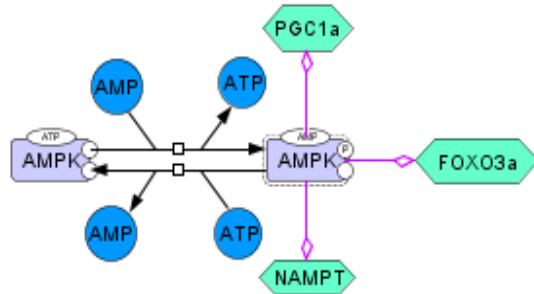


Figure 5: Activation of AMPK requires both a phosphatase and AMP. Once activated, AMPK can phosphorylate many different proteins related to metabolism and oxidative stress regulation.

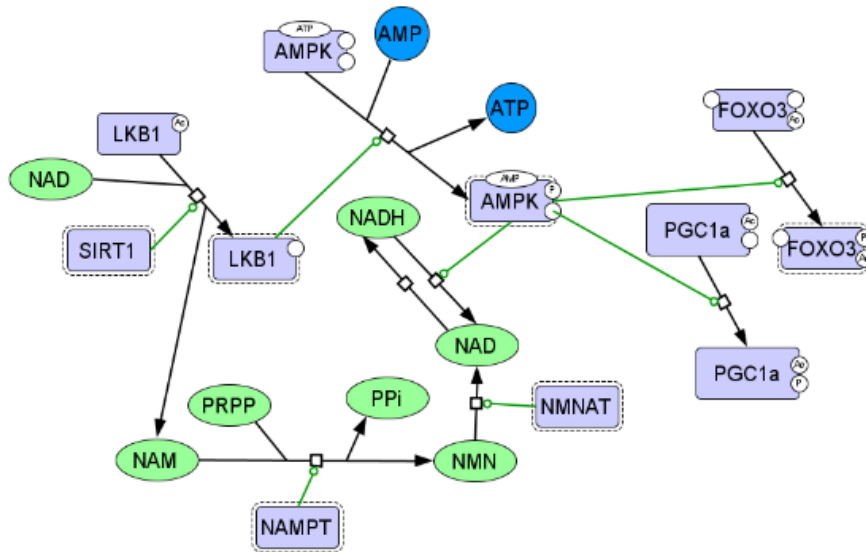


Figure 6: Deacetylation of LKB1 results in AMPK activation under energy deficient conditions (high AMP). Activation of AMPK results in transcription factor activation and changes in metabolic activity increasing in NAD/NADH ratio and SIRT1 activity.

Activation of AMP-activated protein kinase (AMPK) is the transition point from quick modifications of enzyme activity to changes in gene transcription to implement new stress response strategies (Figure 5) (Mihaylova & Shaw, 2011). AMPK activation is dependent on the AMP/ATP ratio, making it an energy sensor. The binding of AMP to AMPK results in increased activity of AMPK. Activation at high AMP/ATP ratios leads to the induction of PGC1 α , FOXO3, and metabolic changes (Figure 6; Hart et al., 2015).

As ROS accumulate in the mitochondria, oxidative damage to the lipid bilayer, proteins and mtDNA will cause cellular stress and dysfunction. If there continues to be an increase in ROS production beyond the capacity of the antioxidant system, mitophagy will be activated and the mitochondria degraded (Mihaylova & Shaw, 2011). When the majority of mitochondria within a cell are dysfunctional, cell death can be initiated to prevent excessive consumption of valuable resources and deleterious signaling from hurting neighboring cells (Lukiw, 2004). This clearance requires changes in gene transcription. For this reason, one of the other targets of SIRT3 is the promoter FOXO3a. SIRT3 deacetylates the protein allowing its export from the mitochondria to the cytosol and further posttranslational modifications which result in changes in mitochondrial gene transcription (Rangarajan et al., 2015).

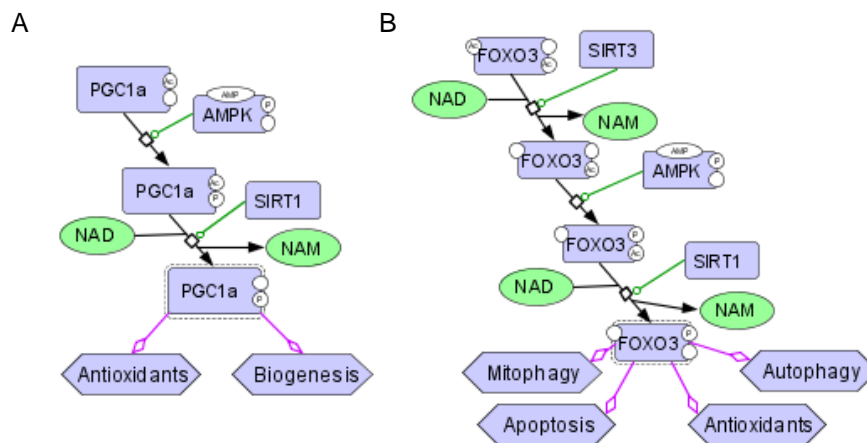


Figure 7A & B: Transcription Factor Activation **A.** PGC1a activation increases antioxidant transcription and mitochondrial biogenesis. **B.** FOXO3a activation leads to mitochondrial degradation as well as increased antioxidant expression.

Before FOXO3a can be activated by AMPK, it must first be deacetylated by SIRT3 in the mitochondria (permitting export to the cytosol), and SIRT1 in the cytosol. Phosphorylation allows for translocation to the nucleus and activation of different transcription factors. PGC1 α is activated by initial deacetylation by SIRT1 in the nucleus

and subsequent phosphorylation by AMPK (Figure 7; Brenmoehl & Hoeflich, 2013; Zrelli, Matsuoka, Kitazaki, Zarrouk, & Miyazaki, 2011). In the nucleus, SIRT1 activates LKB1 via deacetylation. LKB1 can then activate AMPK (Zhang et al., 2018; Figure 6). These pathways are key to the initial response to changes in available glucose, energy and response to metabolic stress and ROS. In turn, these enzymes are regulated by ROS and cofactor levels within the brain. Once activated, FOXO3a will promote the transcription of SOD2, Cat, and different autophagic pathways (Cantó et al., 2009; Hart et al., 2015). Activation of the PGC1 α promoter leads to increased antioxidant and biogenesis enzyme transcription (Figure 7; Sheng et al., 2012). Its gene targets include: SIRT3, PGC1 α , Nrf-1 and nuclear respiratory factors (Nrf-1 and Nrf-2) that lead to changes in ETC and ATP synthase gene expression (Ruetenik & Barrientos, 2015).

Methods

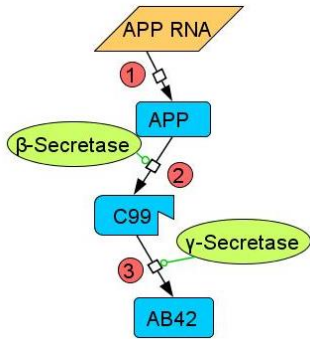
These models were created in CellDesigner 4.2 and converted into a set of ordinary differential equations by SBMLsqueezer (Dräger, Hassis, Supper, Schröder, & Zell, 2008a; Xie, Allaire, & Grolemond, 2019). Model analysis was done in COPASI 4.24.197 (Hoops et al., 2006). Every arrow within the model is represented by a “flux equation.” If the arrow represents formation of the specie, the flux value is positive (Figure 8). If the reaction is using the specie, the reaction will have a negative value. These equations can describe catalyzed and uncatalyzed reactions. If the reaction is not enzyme catalyzed, the flux is described by a simple mass action equation (Equation 1). Like Michaelis-Menten (M-M), the mass action equation also has a rate constant (k_{cat}) but unlike M-M, the overall rate is strictly dependent on the concentration of substrate present. If the reaction is enzyme catalyzed, then the equation takes the form of an M-M equation (2). M-M describes the rate of an enzymatic reaction using two constants. The first describes and enzyme’s binding affinity for its substrate(s), the M-M constant (K_m). The

second describes the maximum rate of the reaction (k_{cat}) (Equation 2). For reactions with more than one substrate, the M-M equation is modified to accommodate a second substrate assuming a random order mechanism (Equation 3). This equation has an additional K_m specific for the second substrate and an inhibition constant (K_i). Like M-M, bi-substrate random order mechanisms assume rapid equilibrium. Under these conditions, $K_{i2}K_{m1} = K_{i1}K_{m2}$ and the latter is simplified out of the final equation (Dräger, Hassis, Supper, Schröder, & Zell, 2008b). These equations are combined to form a series of Flux equations that describe the entire reaction (Figure 8).

$$k_{cat} * [substrate] \tag{1}$$

$$\frac{k_{cat} * [enzyme] * [substrate]}{[substrate] + K_m} \tag{2}$$

$$\frac{k_{cat} * [enzyme] * [s1] * [s2]}{K_{i2} * K_{m1} + [s1] * [s2] + K_{m1} + K_{m2}} \tag{3}$$



$$\begin{aligned} \frac{d([APP] \cdot V_{cell})}{dt} &= +V_{cell} \cdot (k1_{(re1)} \cdot ["APP RNA"]) \\ &\quad - V_{cell} \cdot \left(["B-Secretase"] \cdot \frac{kcat_{re2_s5_{(re2)}} \cdot [APP] \cdot V_{cell}}{kmc_{re2_s2_s5_{(re2)}} + [APP] \cdot V_{cell}} \right) \\ \frac{d(["APP RNA"] \cdot V_{cell})}{dt} &= -V_{cell} \cdot (k1_{(re1)} \cdot ["APP RNA"]) \\ \frac{d([C99] \cdot V_{cell})}{dt} &= +V_{cell} \cdot \left(["B-Secretase"] \cdot \frac{kcat_{re2_s5_{(re2)}} \cdot [APP] \cdot V_{cell}}{kmc_{re2_s2_s5_{(re2)}} + [APP] \cdot V_{cell}} \right) \\ &\quad - V_{cell} \cdot \left(["\gamma-Secretase"] \cdot \frac{kcat_{re3_s7_{(re3)}} \cdot [C99] \cdot V_{cell}}{kmc_{re3_s4_s7_{(re3)}} + [C99] \cdot V_{cell}} \right) \\ \frac{d([AB42] \cdot V_{cell})}{dt} &= +V_{cell} \cdot \left(["\gamma-Secretase"] \cdot \frac{kcat_{re3_s7_{(re3)}} \cdot [C99] \cdot V_{cell}}{kmc_{re3_s4_s7_{(re3)}} + [C99] \cdot V_{cell}} \right) \end{aligned}$$

Figure 8: Flux equations describing the cleavage of APP protein to AB42. Each specie (APP, C99, and AB42) have a differential equation describing the change in concentration over time. Positive equations calculate the production of a specie, negative equations calculate the consumption of a protein.

Concentrations (uM) of proteins were calculated using brain tissue specific abundances from the Pax database and the molecular weights from the Uniprot database (The Uniprot Consortium, 2019; Wang, Herrmann, Simonovic, Szklarczyk, & von Mering,

2015). Metabolite concentrations were taken from the Human Metabolome Database (Wishart et al., 2018). Parameter values were assigned from the BRENDA database (Placzek et al., 2017).

Model Assumptions

SC Assembly

SC assembly is a complex, reactive process of combining respiratory complexes into larger structures. As Late-Onset Alzheimer's Disease is a slow degenerative disease, we followed the MC hypothesis that predicts small differences in RC subunit expression cause a change in respiratory efficiency which can leave neurons more susceptible to inflammation, oxidative damage, and cell death. The SC assembly model investigates how changes in gene expression, determined through proteomic analysis, influence SC assembly and sequestration of CI to reduce ROS formation. The initial model (Figure S1) considers the interactions between four CI subunits and five CIII nuclear encoded subunits not required for ETC function, but required to stabilize the complexes. The stability of the respirasome depends on the expression of associating subunits within each respiratory complex (Lenaz et al., 2010; Ramírez-Camacho et al., 2019). Figure S1 shows that the expression of different subunits, or the loss of subunits, produces respiratory complexes with differing levels of SC stability. Weaker connections cause an increase in ROS production as CI will not be fully stabilized by the SC formation (parameters and equations can be found in the supplement, S3 and S2). When the concentrations of subunits are considered (Table 1), and assuming preference for creating complexes with all of the subunits, S1 is reduced to the model shown in Figure 9.

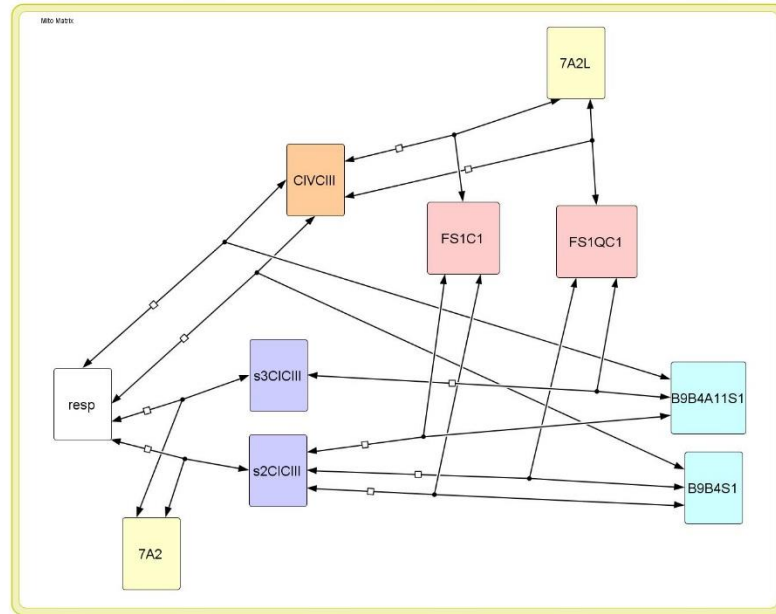


Figure 9: Based on cellular subunit concentrations, the model was reduced to a combination of six complex types that could assemble to form one of three SCs and complete respirasome.

The high concentration of NDUFS1 predicts that assembly favors respirasome formation. Missing one or two subunits results in a weaker association (s2CICIII). When the complexes contain all of the stabilizing subunits, the SC is less likely to disassemble and forms a complete respirasome at a faster rate. The availability of predominant CIV COX7 isoforms COX7A2 and COX7A2L determines whether SC CICIII or CIVCIII will form (Lobo-Jarne et al., 2018).

Antioxidant Model

In living cells, the NAD/NADH pools are linked through the reduction and oxidation of various metabolites to connect glycolysis in the cytosol to energy production in the mitochondria. These two separate pools have differing NAD/NADH ratios to facilitate normal compartment activity, energy production within the mitochondria, and cofactors in the cytosol. AMPK also regulates the NAD/NADH ratio in the cytosol, as it does *in vivo*

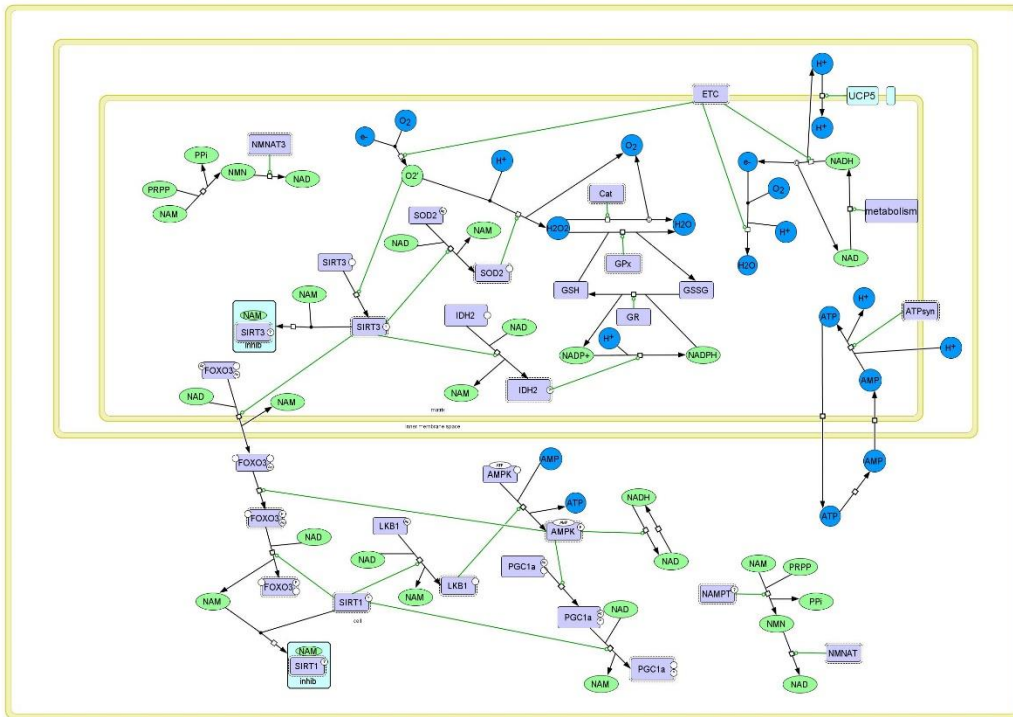


Figure 10: The mitochondria model being simulated to test analyze the activation of transcription factors and antioxidant system capacity.

(Cantó et al., 2009). In this model, we assumed that the two pools were separate and that the local changes in the NAD/NADH ratios are only changing in response to respiratory activity, ROS production and AMPK-mediated metabolic changes. ATP consumption was also generalized to hydrolysis of ATP to AMP rather than ADP. Though both do happen, the simplification to only show ATP and AMP levels was done to show ATP consumption as well as activation of AMPK through AMP binding. The ETC concentration is also assumed due to stable complexes not missing subunits.

Parameter Optimization

The final parameter set for the oxidative stress models was found by providing an initial parameter set. This set was created based on rate constants found in the BRENDA database. Those that could not be found were given an initial value of 0.01 for Km and 1

for k_{cat} . The initial and final parameter sets can be found in the supplement (S7 and S6). Parameter units for k_{cat} , and K_m are min^{-1} and μM respectively. This set underwent an optimization using the Hooke and Jeeves solver in COPASI to produce the final parameter set. These adjusted values better illustrate true pathway activity.

Sensitivity data

A sensitivity analysis (SA) of the oxidative stress model was performed to quantify sensitive points within the model system. The task perturbs one specie concentration by 1%, and COPASI records how this change effects the dependent variables of the system (reaction rates and transient concentrations). The results are presented as the average percent dependency of a dependent variable's value on the initial concentration being varied. This analysis is only accurate for perturbations up to 5%, higher changes in concentration deviate from the predicted trend.

Treatment Tests

Treatment data was determined using COPASI's time course analysis. Each treatment mimics the effects of CRISPR-Cas type gene therapy and was done by adjusting the protein concentration up or down 50%. Steps of 0.1 minutes were used to record transient concentration values over the course of a 100 minute simulations. Most data is presented as the percent difference between the control model and the treatment model. Calculations and graphing were done in RStudio (3.5.2) by finding the difference between treatment (up or down regulation) groups and the control then dividing by the control concentration and multiplying by 100.

Results

The two models produced data explaining different aspects of mitochondrial dysfunction and potential treatment directions. The SC assembly model demonstrates how differences in AD and healthy gene expression can change the concentration of SC's

and respirasomes in the cells which has wider impacts on mitochondrial efficiency. The oxidative stress model shows that an increase in ROS due to structural or other changes in SC content and formation observed in the SC assembly model can impact the activation of transcription factors. Together these therapeutic tests provide valuable information on how changes in subunit or enzyme expression can influence further changes in gene transcription in response to superoxide production.

SC Assembly Results

The formation of SC's varies between cell types and is implicated in ROS production (Acin-Perez & Enriquez, 2014). The uniqueness of SC formation to cell types predicts that changes in assembly will have widespread effects on mitochondrial and subsequently cellular homeostasis. To understand how AD affects respirasome formation and to grow intuition about how increasing subunit expression can either alleviate or exacerbate these issues, we simulated SC formation in control and AD conditions. After compiling specie concentrations, the fold regulations from Dr. Castora's work was used to determine the AD concentrations (Table 1). The values were then loaded into the model assuming that only one subunit could be absent from a functional complex. There is an overall decrease in available subunits including a decrease of approximately 2-fold in essential respirasome assembly subunit NDUFS1.

After determining AD ETC concentrations, treatment sets were created by increasing one subunit concentration by 50% relative to AD concentrations. The concentration of individual complexes was reassessed with the treatment and shown in Table 2. The treatment sets were analyzed for how they affected CI stability via assembly with CIII and CIV. CIII is an important initial CI binding partner with CIV providing minor additional stability after CICIII formation (Lobo-Jarne et al., 2018). Subunit targets were

1 (uM)	Control	AD
<i>UQCRFS1</i>	13.62	7.41
<i>UQCRC1</i>	9.57	3.75
<i>UQCRQ</i>	5.14	2.49
<i>NDUFB9</i>	7.42	2.52
<i>NDUFB4</i>	10.06	9.22
<i>NDUFA11</i>	1.85	0.84
<i>NDUFS1</i>	6.29	2.44
<i>COX7A2L</i>	3.54	2.04
<i>COX7A2</i>	28.63	13.39

Table 1: Control and AD tissue ETC subunit concentrations given in uM. Complex abbreviations: UQCR- CIII, NDUF- CI, COX- CIV

2 (uM)	Control	AD	UQCRC1	UQCRQ	NDUFA11	NDUFS1	NDUFB9
<i>CI</i>							
<i>B9B4A11S1</i>	1.85	0.84	0.84	0.84	1.26	0.84	0.84
<i>B9B4S1</i>	4.44	1.60	1.60	1.60	1.18	2.83	2.93
<i>CIII</i>							
<i>FS1QC1</i>	5.15	2.49	2.49	3.73	2.49	2.49	2.49
<i>FS1C1</i>	2.72	1.26	3.13	0.02	1.26	1.26	1.26

Table 2: Initial concentrations of individual complexes based on control, AD and treatment subunit concentrations. Treatment sets were created by increasing one subunits concentration by 50%. Subunits that did not increase or decrease the concentration of complexes were not considered

selected based on their effect on CI or CIII concentrations compared to AD values. Simulations of SC assembly produced information about changes in respirasome concentration (Figure 11) and changes in the percent of CI: free CI, and sequestered by CICIII or respirasomes (Figure 12). The percentage of free CI in the AD sample is double that of the control, and the decreased respirasome formation (Figure 11 & 12) indicates that the AD tissue underwent a long period of oxidative stress. The CI subunit treatments

11 Respirasome concentration

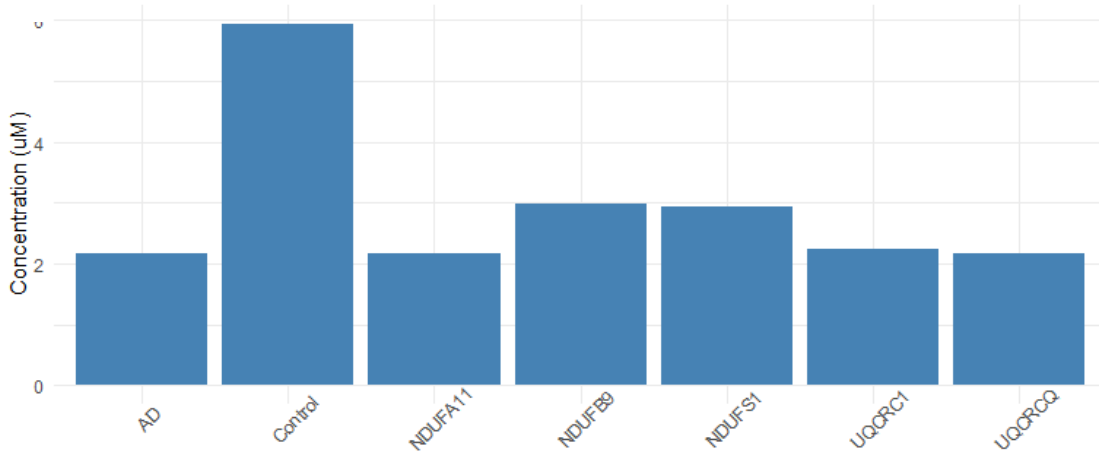


Figure 11: Respirasome concentration (uM) in the control, AD, and treatment groups

12 Incorporation of CI into SC's

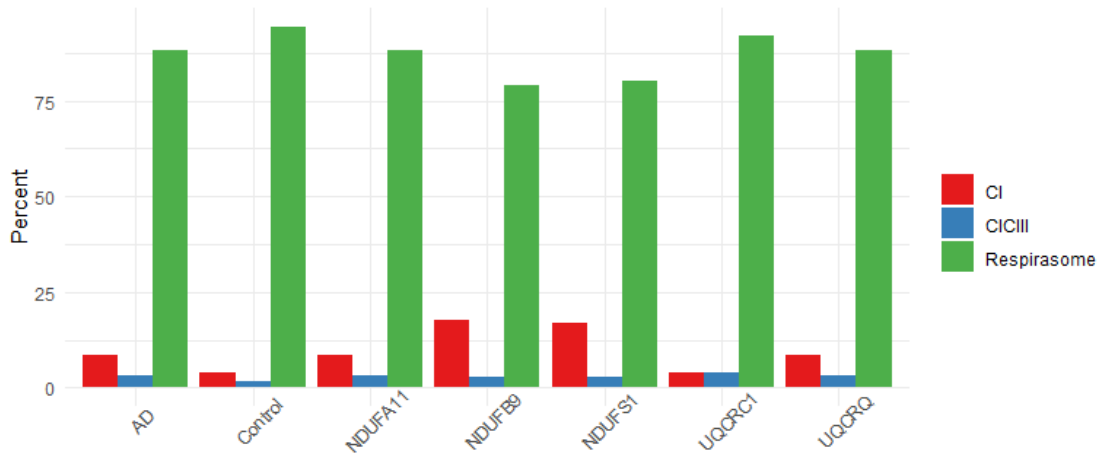


Figure 12: Percent of CI assembled into SCs (blue) respirasomes (green) or free (red) in control and treatment groups.

predict that increasing respirasome concentration comes with an increase in free CI and potentially dangerous levels of ROS production. NDUF51 and NDUFB9 treatments were able to increase the concentration of respirasome (Figure 12), but this increase in respirasome concentration was paralleled by an increase in free CI. UQCRC1 treatment was the only therapy predicted to increase respirasome formation and CI sequestration and ultimately a decreased percentage of free CI. Based on this model, we predict that

targeting increased CIII binding to CI and not increasing available CI for respirasome binding is a viable treatment strategy to increase sequestration of CI and reduce ROS production related to CI activity.

Oxidative Stress Model Results

3	ETC	Metabolic	SIRT3	ATPsyn
Concentration Sensitivity				
NADH	-3.408	3.428	0.000	0
O2 Radicals	0.003	0.563	0.000	0
NADPH	-0.013	-2.142	0.000	0
Glutathione Dimer	0.003	0.996	0.000	0
Flux Sensitivity				
Exported FOXO3	0.000	0.004	0.078	0
Peroxide Formation	0.003	0.990	0.000	0
e- capture	1.002	0.982	-0.016	0
GSSG reduction	0.003	0.990	0.000	0
FOXO3 export	0.000	0.006	0.130	0

Table 3: Scaled SA analysis of the oxidative stress model to perturbations in therapy target species ETC, Metabolic Enzymes, SIRT3, and ATP synthase. **Upper:** sensitivity of key model species concentrations. **Lower:** Sensitivity of reaction fluxes to perturbations

Mitochondrial biogenesis is a delicate process facilitating mitochondrial activity through increased antioxidant and mitochondrial subunit expression in response to changes in ATP and ROS production. When energy production cannot be salvaged and continual oxidative stress places the cell at risk of apoptosis, these response pathways activate autophagy and mitophagy. Our results predict that metabolic activity, ETC stability and electron saturation play important roles in ROS generation and mitochondrial oxidative stress. SIRT1 and AMPK are also an important for sending extra-mitochondrial stress signals which activate and transport transcription factors.

An SA of the oxidative stress model was done to assess potential therapeutic targets. The analysis predicted that increased stable ETC, changes in metabolic enzymes

and increased SIRT3 protein will decrease superoxide accumulation or activate the oxidative stress response. It also predicts that treatments dealing with ETC and metabolic enzyme concentrations will have opposing effects (Table 3). Increased metabolic activity meant that NADH levels increased, providing more substrate for energy production. However, as the literature also shows (Pryde & Hirst, 2011), increased availability of NADH is linked to heightened superoxide levels as the ETC and CoQ pools become more reduced. The high levels of reduced ETC and CoQ lead to reverse electron transport and an increased potential for oxygen binding to CI. Both of these facilitate superoxide production. An increase in NADH can also dampen the ability of SIRT3 to increase antioxidant activity and activate FOXO3 export from the mitochondria. Decreased levels of NADPH and increasing glutathione dimers also indicate that changes in the metabolic activity affect the overall redox state of the mitochondria (Table 3). The minimal change in GSSG reduction and increased FOXO3 export indicate a higher level of stress and subsequent activation of a stress response. Low changes in superoxide with increased stable ETC is in agreement with the literature (Ramírez-Camacho et al., 2019) that CI saturation with electrons (from NADH) leads to increased superoxide production. Higher levels of stable ETC complexes results in a lower percentage of these complexes existing in a reduced state. This limits the potential production of superoxide. Within the model, increasing the ETC did not change peroxide production (a common marker of superoxide production) compared to the control. As small amounts of peroxide production are important for normal mitochondrial signaling, if the SA results hold true at perturbations at higher than 1% this provides a promising avenue for targeting SC stability for AD treatment.

The SA indicated that metabolic enzymes had a negative effect on the model. Therefore, when considering treatments, we tested a 50% decrease in metabolic enzymes, as well as a 50% increase in SIRT3 and stable ETC. After an initial spike in activity related to beginning the model simulation, there is no change in superoxide production by the ETC while the metabolic enzyme treatment decreased superoxide production (Figure 13). As a certain level of peroxide is necessary for normal cell function, the benefits of metabolic enzyme treatment are likely highly sensitive to the exact enzymes and pathways being targeted.

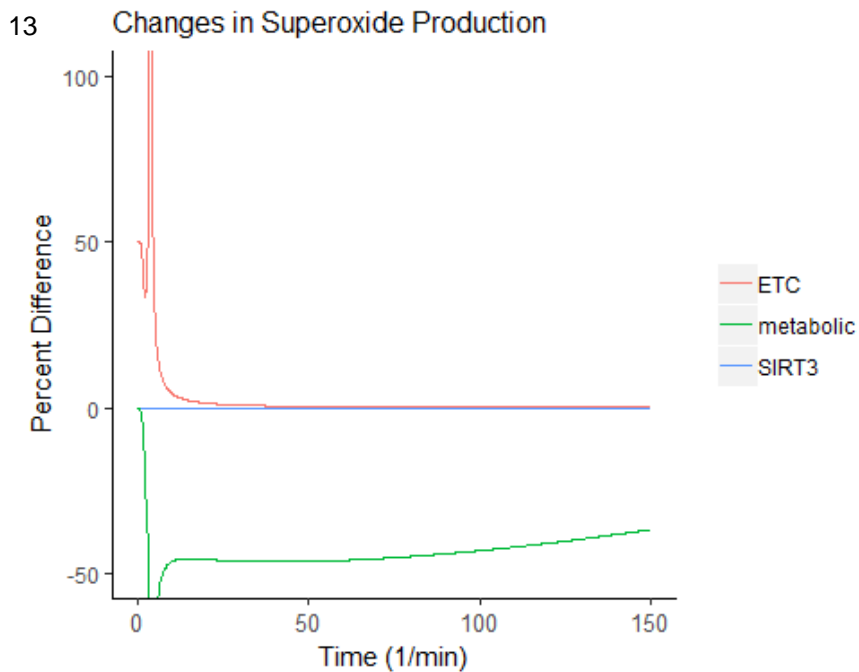


Figure 13: Percent difference in superoxide production compared to control. Therapy targets ETC and SIRT3 do not make a long term impact on the production of superoxide. Theoretical metabolic enzyme therapy reduces the superoxide production by approximately 50%

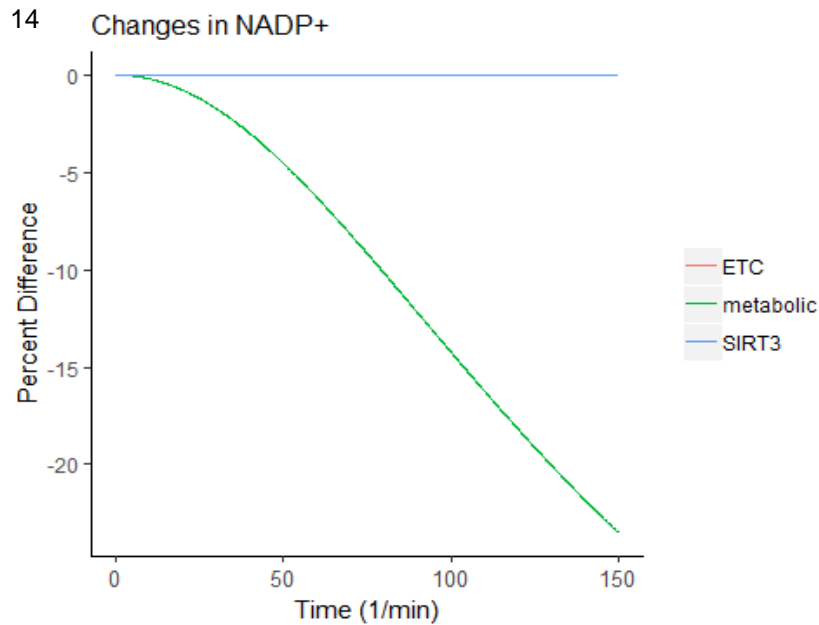


Figure 14: Percent change in NADP⁺ concentration with ETC, metabolic enzyme and SIRT3 treatment compared to control.

The decreasing NADP⁺ concentration with metabolic treatment (Figure 14) demonstrates that the antioxidant cofactor is becoming more reduced with treatment and the mitochondria then has a heightened ability to eliminate ROS. As with superoxide production shown in Figure 13, the ETC stabilizing treatment does not affect NADPH levels. Another aspect of mitochondrial function is the availability of NAD and NADH. The NAD/NADH ratio governs metabolic activity and influences antioxidant cofactor availability. The control NAD/NADH ratio in this model is high compared to that found in living systems, but it is proportionally smaller than the cytoplasmic ratio as seen in the same living systems. Increasing SIRT3 made no difference in the NAD/NADH ratio despite use of NAD as a cofactor. For drug targets aimed to increase antioxidant activity, this is important as it predicts minimal unanticipated effects on normal mitochondrial activity.

4	AMPK	LKB1	SIRT1
<i>Concentration Sensitivities</i>			
<i>PGC1α</i>	0.000	0.000	0.001
<i>FOXO3</i>	0.029	0.001	0.578
<i>NAD/NADH</i>	0.587	0.346	0.003
<i>Flux Sensitivities</i>			
<i>NAM to NMN</i>	0.026	0.022	0.587
<i>AMPK activation</i>	0.000	0.481	0.587
<i>NADH oxidation</i>	0.016	0.009	0.000

Table 4: Cytosolic Target SA **Upper:** Sensitivities of active transcription factor concentration and NAD/NADH ratio to targets AMPK, LKB1 and SIRT1. **Lower:** Sensitivities of reaction fluxes to perturbations in enzyme concentrations.

This predicts that increased SIRT activity may be a way of strengthening mitochondrial stress response without interfering with normal respiratory activity. Consistent with Figure 15 and Table 4, decreasing metabolic enzymes had a beneficial impact on the NAD/NADH ratio. Increasing stable ETC leads to a notably higher ratio. This higher ratio favors activation of antioxidant pathways which can decompose any stress-related increases in superoxide not handled by the decreased demand and oxidation of the individual complexes.

The SAs of cytosolic therapy targets highlight important relationships between the signaling pathways, feedback loops and transcription factor activation. Both AMPK and LKB1 had a minor impact on PGC1 α and FOXO3 activation (Table 4), but were able to increase the flux of NMN synthesis, an indicator of SIRT1 activity and the AMPK positive feedback loop. The sensitivity of active FOXO3 to SIRT1 concentrations indicates that SIRT1 is important for FOXO3 activation. However, there is potential for AMPK treatment to increase the positive feedback loop with SIRT1 to increase FOXO3 activation. The

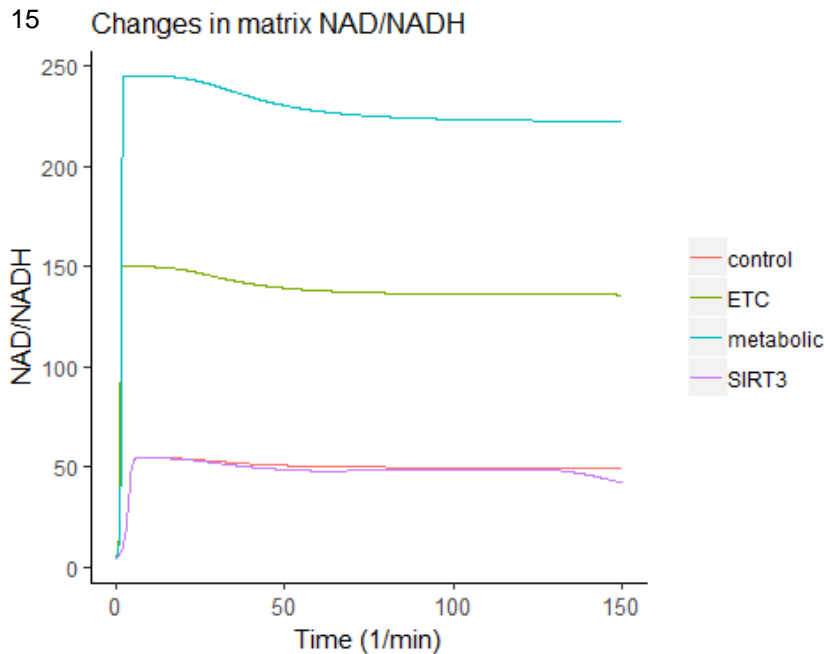


Figure 15: Changes in mitochondrial NAD/NADH ratios with target treatments. Metabolic enzyme treatment (blue) made the largest impact on the NAD/NADH ratio. The stabilized ETC treatment (green) caused the ratio to triple while SIRT3 treatment (purple) did not change the NAD/NADH ratio

correlation between AMPK activity and the NAD/NADH ratio (Table 4) results in the beneficial increase in SIRT1 activity shown by the increase in nicotinamide (NAM).

The cytosolic reactions shown in this model are only in response to oxidative stress. They are analyzed for changes in transcription factor activation. PGC1 α and FOXO3 both require SIRT1 deacetylation and AMPK phosphorylation to enter the nucleus. The activity of these proteins is increased with increasing oxidative stress *in vitro* (Duan et al., 2016), but this model shows a preferential activation of FOXO3 (Figure 16). There was no change in ATP/AMP ratio.

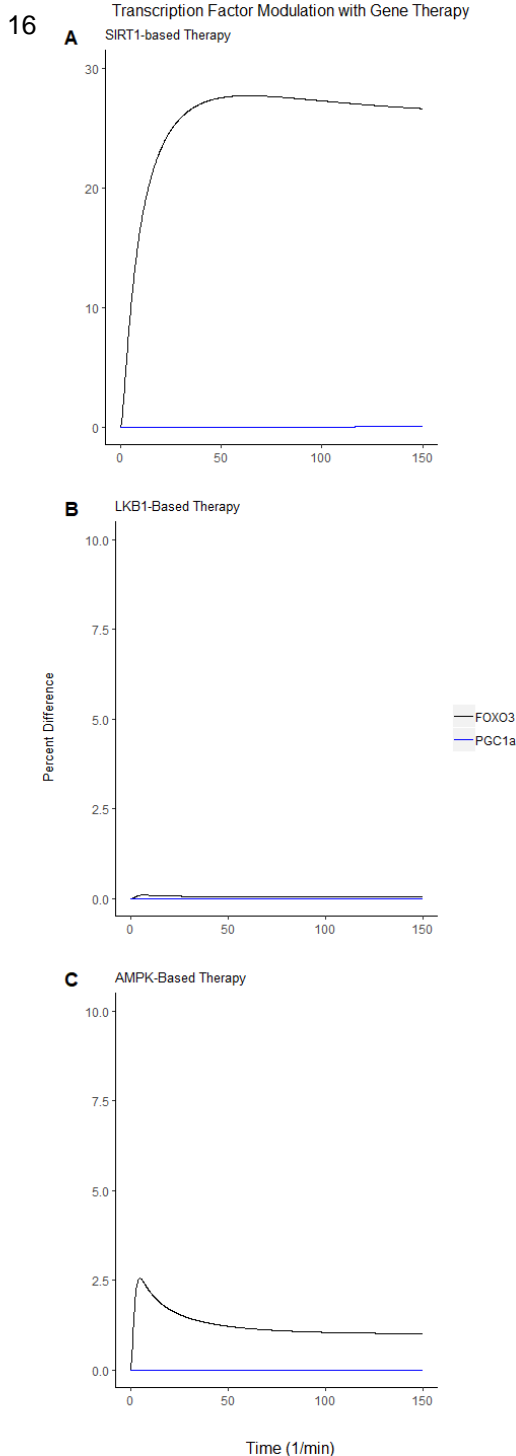


Figure 16: Transcription factor activation with therapy targets SIRT1 (A), LKB1 (B), and AMPK (C). The model predicts that FOXO3 will be preferentially activated by changes in ROS production. AMPK and SIRT1 are the most effective treatment options.

The model predicted that FOXO3 is preferentially activated by oxidative stress. The lack of PGC1 α activation indicates that it is more sensitive to ATP availability and production which deactivates AMPK. SIRT1 is predicted to be the more effective therapeutic target due to the changes in the FOXO3a activation and its widespread impact on autophagy activation (Figure 16). AMPK is a second potential target. It plays an important role in both FOXO3 and PGC1 α activation, but the low PGC1 α activation in this model hints that changes in ATP availability may be more important for PGC1 α activation than FOXO3. Depending on the goal of therapy (eliminate dysfunctional mitochondria or restore respiratory activity) different targets should be considered.

Discussion

The MC hypothesis predicts that deficits in respiratory chain efficiency lead to ROS accumulation as we age and predisposes individuals to the onset of

neurodegenerative diseases (Mosconi, 2013). The work of Dr. Castora's lab complements this hypothesis, showing that there are changes in respiratory chain gene expression levels in individuals with AD. Using this information on gene expression, we created two models investigating the impacts such differences can have in respiratory function and subsequent stress-related signaling. ROS production increases the activity of SIRT3, SOD2, Cat, and Gpx to prevent oxidative damage to surrounding tissues and mitochondrial DNA (Ighodaro & Akinloye, 2017). If this constitutive antioxidant system cannot reduce ROS, SIRT3 activates a signaling cascade inducing FOXO3 and PGC1 α mediated transcription of antioxidant and autophagic genes (Brenmoehl & Hoeflich, 2013). Specific transcription factor activation is important for disease onset and well as mitigation. By activating the correct transcription factor, we can direct activation of beneficial pathways and prevent the activation of detrimental pathways. This model predicts that ROS production does not directly affect ATP production, but preferentially activates the FOXO3 transcription factor. Therefore, a decrease in ATP resulting from lower respiratory activity better activates AMPK, initiating PGC1 α activation and mitochondrial biogenesis. As FOXO3 transcriptional targets activates autophagy as well as antioxidant proteins, this avenue of treatment should be considered with caution. Moderate increases in activity will likely activate the clearance of ROS and dysfunctional mitochondria, but if changes are too large they can result in a hyperactive autophagy pathway which is more cytotoxic than neuroprotective. SIRT1 is a viable target as it is predicted to be important for both FOXO3 and PGC1 α activation. AMPK would be effective in upregulating PGC1 α and increasing mitochondrial biogenesis inducing the feedback loop to SIRT1 activation. Picking AMPK-related targets may also provide more balance between FOXO3 and PGC1 α activation to prevent conservation of irreversibly dysfunctional mitochondria that put the entire neuron at risk.

Respiratory and metabolic targets present a safer therapeutic avenue. By picking targets that increase stable SC formation, we can decrease ROS production at its root with fewer risks of aberrant pathway or signaling changes. CIIII formation is the most important step in reducing CI related ROS production. By covering one of two oxygen binding sites as well as increasing CI binding partners, CIII subunit UQCRC1 is predicted to be the most effective subunit target. The model shadowed this prediction as seen in the increase in CI sequestered within SC's.

These model predictions about transcription factor activation and SC assembly may be of importance when understanding the mitochondrial differences between elder and long-lived individuals. People who live to be older than 75 years have defective mitochondria with high peroxide concentrations and low ATP levels (Sgarbi et al., 2014). The results of this model would predict that this unique trait may be due to sequential changes in gene transcription allowing for mitochondrial fusion (changes in bioenergetics) before autophagy activation. This sequence could prevent autophagic degradation because the hyperfusion of mitochondria make them resistant to degradation. It is unclear how this adaptation relates to AD, but the correlation with lifespan is favorable. Further work studying the effects of subunit and antioxidant therapies on mitochondrial stress response *in vitro* to assess the utility of these treatments is required to confirm these predictions.

References

- Acin-Perez, R., & Enriquez, J. A. (2014). The function of the respiratory supercomplexes: The plasticity model. *Biochimica et Biophysica Acta (BBA) - Bioenergetics*, 1837(4), 444–450. <https://doi.org/10.1016/J.BBABIO.2013.12.009>
- Acín-Pérez, R., Fernández-Silva, P., Peleato, M. L., Pérez-Martos, A., & Enriquez, J. A. (2008). Respiratory Active Mitochondrial Supercomplexes. *Molecular Cell*, 32(4), 529–539. <https://doi.org/10.1016/J.MOLCEL.2008.10.021>
- Arthur, C. R., Morton, S. L., Dunham, L. D., Keeney, P. M., & Bennett, J. P. (2009). Parkinson's disease brain mitochondria have impaired respirasome assembly, age-related increases in distribution of oxidative damage to mtDNA and no differences in heteroplasmic mtDNA mutation abundance. *Molecular Neurodegeneration*, 4(1), 37. <https://doi.org/10.1186/1750-1326-4-37>
- Bechtel, W., & Bauer, G. (2009). Catalase protects tumor cells from apoptosis induction by intercellular ROS signaling. *Anticancer Research*, 29(11), 4541–4557. <https://doi.org/29/11/4541> [pii]
- Blacker, T. S., & Duchon, M. R. (2016). Investigating mitochondrial redox state using NADH and NADPH autofluorescence. *Free Radical Biology and Medicine*, 100, 53–65. <https://doi.org/10.1016/j.freeradbiomed.2016.08.010>
- Brenmoehl, J., & Hoeflich, A. (2013). Dual control of mitochondrial biogenesis by sirtuin 1 and sirtuin 3. *Mitochondrion*, 13(6), 755–761. <https://doi.org/10.1016/j.mito.2013.04.002>
- Cadenas, E., & Davies, K. J. A. (2000). MITOCHONDRIAL FREE RADICAL GENERATION, OXIDATIVE STRESS, AND AGING. *Radical Biology & Medicine*, 29(3/4), 222–230. [https://doi.org/0891-5849/00/\\$](https://doi.org/0891-5849/00/$)
- Cai, Z., Yan, L.-J., Li, K., Quazi, S. H., & Zhao, B. (2012). Roles of AMP-activated Protein Kinase in Alzheimer's Disease. *NeuroMolecular Medicine*, 14(1), 1–14. <https://doi.org/10.1007/s12017-012-8173-2>
- Campion, D., Dumanchin, C., Hannequin, D., Dubois, B., Belliard, S., Puel, M., ... Frebourg, T.

- (1999). Early-Onset Autosomal Dominant Alzheimer Disease: Prevalence, Genetic Heterogeneity, and Mutation Spectrum. *The American Journal of Human Genetics*, 65(3), 664–670. <https://doi.org/10.1086/302553>
- Cantó, C., Gerhart-Hines, Z., Feige, J. N., Lagouge, M., Noriega, L., Milne, J. C., ... Auwerx, J. (2009). AMPK regulates energy expenditure by modulating NAD⁺ metabolism and SIRT1 activity Europe PMC Funders Group. *Nature*, 458(7241), 1056–1060. <https://doi.org/10.1038/nature07813>
- Carlberg, I., & Mannervik, B. (1975). Purification and characterization of the flavoenzyme glutathione reductase from rat liver. *The Journal of Biological Chemistry*, 250(14), 5475–5480. Retrieved from <http://www.ncbi.nlm.nih.gov/pubmed/237922>
- Chen, Y., Zhang, J., Lin, Y., Lei, Q., Guan, K. L., Zhao, S., & Xiong, Y. (2011). Tumour suppressor SIRT3 deacetylates and activates manganese superoxide dismutase to scavenge ROS. *EMBO Reports*, 12(6), 534–541. <https://doi.org/10.1038/embor.2011.65>
- Demetrius, L. A., & Simon, D. K. (2013). The inverse association of cancer and Alzheimer's: a bioenergetic mechanism. *Journal of The Royal Society Interface*, 10(82), 20130006–20130006. <https://doi.org/10.1098/rsif.2013.0006>
- Dräger, A., Hassis, N., Supper, J., Schröder, A., & Zell, A. (2008a). SBMLsqueezer: A CellDesigner plug-in to generate kinetic rate equations for biochemical networks. *BMC Systems Biology*, 2(1), 39. <https://doi.org/10.1186/1752-0509-2-39>
- Dräger, A., Hassis, N., Supper, J., Schröder, A., & Zell, A. (2008b). SBMLsqueezer: Kinetic Laws. *University of Tubingen*. Retrieved from https://static-content.springer.com/esm/art%3A10.1186%2F1752-0509-2-39/MediaObjects/12918_2007_196_MOESM1_ESM.pdf
- Du, H., & Yan, S. S. Du. (2010). Mitochondrial permeability transition pore in Alzheimer's disease: Cyclophilin D and amyloid beta. *Biochimica et Biophysica Acta - Molecular Basis of Disease*, 1802(1), 198–204. <https://doi.org/10.1016/j.bbadis.2009.07.005>
- Duan, W.-J., Li, Y.-F., Liu, F.-L., Deng, J., Wu, Y.-P., Yuan, W.-L., ... He, R.-R. (2016). A

- SIRT3/AMPK/autophagy network orchestrates the protective effects of trans-resveratrol in stressed peritoneal macrophages and RAW 264.7 macrophages. *Free Radical Biology*, 95, 230–242. <https://doi.org/10.1016/j.freeradbiomed.2016.03.022>
- Feldman, J. L., Dittenhafer-Reed, K. E., & Denu, J. M. (2012). Sirtuin Catalysis and Regulation. *THE JOURNAL OF BIOLOGICAL CHEMISTRY*, 276(51), 42419–42427. <https://doi.org/10.1074/jbc.R112.378877>
- Greggio, C., Jha, P., Kulkarni, S. S., Lagarrigue, S., Broskey, N. T., Boutant, M., ... Amati, F. (2017). Enhanced Respiratory Chain Supercomplex Formation in Response to Exercise in Human Skeletal Muscle. *Cell Metabolism*, 25(2), 301–311. <https://doi.org/10.1016/J.CMET.2016.11.004>
- Grimm, A., Friedland, K., & Eckert, A. (2016). Mitochondrial dysfunction: the missing link between aging and sporadic Alzheimer's disease. *Biogerontology*, 17(2), 281–296. <https://doi.org/10.1007/s10522-015-9618-4>
- Guan, X., Lin, P., Knoll, E., & Chakrabarti, R. (2014). Mechanism of Inhibition of the Human Sirtuin Enzyme SIRT3 by Nicotinamide: Computational and Experimental Studies. *Computational and Experimental Studies*, 9(9). <https://doi.org/10.1371/journal.pone.0107729>
- Hart, P. C., Mao, M., De Abreu, A. L. P., Ansenberger-Fricano, K., Ekoue, D. N., Ganini, D., ... Bonini, M. G. (2015). MnSOD upregulation sustains the Warburg effect via mitochondrial ROS and AMPK-dependent signalling in cancer. *Nature Communications*, 6, 1–14. <https://doi.org/10.1038/ncomms7053>
- Herrup, K. (2015). The case for rejecting the amyloid cascade hypothesis. *Nature Neuroscience*, 18(6), 794–799. <https://doi.org/10.1038/nn.4017>
- Hoops, S., Sahle, S., Gauges, R., Lee, C., Pahle, J., Simus, N., ... Kummer, U. (2006). COPASI-- a COmplex PAtchway Simulator. *Bioinformatics*, 22(24), 3067–3074. <https://doi.org/10.1093/bioinformatics/btl485>
- Ighodaro, O. M., & Akinloye, O. A. (2017). First line defence antioxidants-superoxide dismutase (SOD), catalase (CAT) and glutathione peroxidase (GPX): Their fundamental role in the entire

- antioxidant defence grid. *Alexandria Journal of Medicine*, 1–7.
<https://doi.org/10.1016/j.ajme.2017.09.001>
- Kim, G. H., Kim, J. E., Rhie, S. J., & Yoon, S. (2015). The Role of Oxidative Stress in Neurodegenerative Diseases. *Experimental Neurobiology*, 24(4), 325.
<https://doi.org/10.5607/en.2015.24.4.325>
- Kincaid, B., & Bossy-Wetzell, E. (2013). Forever young: SIRT3 a shield against mitochondrial meltdown, aging, and neurodegeneration. *Frontiers in Aging Neuroscience*, 5, 48.
<https://doi.org/10.3389/fnagi.2013.00048>
- Lambert, A. J., & Brand, M. D. (2004). *Superoxide production by NADH:ubiquinone oxidoreductase (complex I) depends on the pH gradient across the mitochondrial inner membrane. Biochem. J* (Vol. 382). Retrieved from <http://www.biochemj.org/content/ppbiochemj/382/2/511.full.pdf>
- Lapuente-Brun, E., Moreno-Loshuertos, R., Acín-Pérez, R., Latorre-Pellicer, A., Colás, C., Balsa, E., ... Enríquez, J. A. (2013). Supercomplex Assembly Determines Electron Flux in the Mitochondrial Electron Transport Chain. *Science*, 340(6140), 1567–1570.
<https://doi.org/10.1126/SCIENCE.1230381>
- Lenaz, G., Baracca, A., Barbero, G., Bergamini, C., Dalmonte, M. E., Del Sole, M., ... Solaini, G. (2010). Mitochondrial respiratory chain super-complex I–III in physiology and pathology. *Biochimica et Biophysica Acta (BBA) - Bioenergetics*, 1797(6–7), 633–640.
<https://doi.org/10.1016/J.BBABIO.2010.01.025>
- Letts, J. A., Fiedorczuk, K., & Sazanov, L. A. (2016). The architecture of respiratory supercomplexes. *Nature*, 537(7622), 644–648. <https://doi.org/10.1038/nature19774>
- Ling Liu, X. S., William J. Quinn III, ..., Timothy J. Mitchison, Joseph A. Baur, & Joshua D. Rabinowitz. (2018). Quantitative Analysis of NAD Synthesis-Breakdown Fluxes. *Cell Metabolism*, 27, 1067–1080. <https://doi.org/https://doi.org/10.1016/j.cmet.2018.03.018>
- Liu, S.-H., Huang, J.-P., Lee, R. K.-K., Huang, M.-C., Wu, Y.-H., Chen, C.-Y., & Chen, C.-P. (2010). Paracrine Factors from Human Placental Multipotent Mesenchymal Stromal Cells Protect Endothelium from Oxidative Injury via STAT3 and Manganese Superoxide Dismutase

- Activation1. *Biology of Reproduction*, 82(5), 905–913.
<https://doi.org/10.1095/biolreprod.109.081828>
- Lobo-Jarne, T., Nývltová, E., Pérez-Pérez, R., Timón-Gómez, A., Molinié, T., Choi, A., ... Barrientos, A. (2018). Human COX7A2L Regulates Complex III Biogenesis and Promotes Supercomplex Organization Remodeling without Affecting Mitochondrial Bioenergetics. *Cell Reports*, 25(7), 1786–1799.e4. <https://doi.org/10.1016/j.celrep.2018.10.058>
- Lopez-Fabuel, I., Le Douce, J., Logan, A., James, A. M., Bonvento, G., Murphy, M. P., ... Bolaños, J. P. (2016). Complex I assembly into supercomplexes determines differential mitochondrial ROS production in neurons and astrocytes. *Proceedings of the National Academy of Sciences of the United States of America*, 113(46), 13063–13068.
<https://doi.org/10.1073/pnas.1613701113>
- Lukiw, W. J. (2004). Gene Expression Profiling in Fetal, Aged, and Alzheimer Hippocampus: A Continuum of Stress-Related Signaling*. *Neurochemical Research*, 29(6), 1287–1297.
Retrieved from <https://link.springer.com/content/pdf/10.1023%2FB%3ANERE.0000023615.89699.63.pdf>
- Mancuso, M., Orsucci, D., Siciliano, G., & Murri, L. (2008). Mitochondria, mitochondrial DNA and Alzheimer's disease. What comes first? *Current Alzheimer Research*, 5(5), 457–468.
Retrieved from <http://www.ncbi.nlm.nih.gov/pubmed/18855587>
- Maranzana, E., Falasca, A., Barbero, G., Falasca, A. I., Lenaz, G., & Genova, M. L. (2013). Mitochondrial Respiratory Supercomplex Association Limits Production of Reactive Oxygen Species from Complex I. *Antioxid. Redox Signal*, 19, 1469–1480.
<https://doi.org/10.1089/ars.2012.4845>
- Mihaylova, M. M., & Shaw, R. J. (2011). The AMP-activated protein kinase (AMPK) signaling pathway coordinates cell growth, autophagy, & metabolism. *Nature Cell Biology*, 13(2011), 1016–1023. <https://doi.org/10.1038/ncb2329>
- Milenkovic, D., Blaza, J. N., Larsson, N.-G., & Hirst, J. (2017). The Enigma of the Respiratory Chain Supercomplex. *Cell Metabolism*, 25(4), 765–776.

<https://doi.org/10.1016/J.CMET.2017.03.009>

Mosconi, L. (2013). Glucose metabolism in normal aging and Alzheimer's disease: Methodological and physiological considerations for PET studies. *Clinical and Translational Imaging*, 1(4).

<https://doi.org/10.1007/s40336-013-0026-y>

Murphy, M. P. (2009). How mitochondria produce reactive oxygen species. *Biochemical Journal*, 417(1), 1–13. <https://doi.org/10.1042/BJ20081386>

Nikiforov, A., Dölle, C., Niere, M., & Ziegler, M. (2011). Pathways and subcellular compartmentation of NAD biosynthesis in human cells: From entry of extracellular precursors to mitochondrial NAD generation. *Journal of Biological Chemistry*, 286(24), 21767–21778.

<https://doi.org/10.1074/jbc.M110.213298>

Ogura, Y., Kitada, M., Monno, I., Kanasaki, K., Watanabe, A., & Koya, D. (2018). Renal mitochondrial oxidative stress is enhanced by the reduction of Sirt3 activity, in Zucker diabetic fatty rats. *Redox Report*, 23(1), 153–159. <https://doi.org/10.1080/13510002.2018.1487174>

Placzek, S., Schomburg, I., Chang, A., Jeske, L., Ulbrich, M., Tillack, J., & Schomburg, D. (2017). BRENDA in 2017: new perspectives and new tools in BRENDA. *Nucleic Acids Research*, 45.

<https://doi.org/10.1093/nar/gkw952>

Pryde, K. R., & Hirst, J. (2011). Superoxide Is Produced by the Reduced Flavin in Mitochondrial Complex I. *THE JOURNAL OF BIOLOGICAL CHEMISTRY*, 286(20), 18056–18065.

<https://doi.org/10.1074/jbc.M110.186841>

Ramírez-Camacho, I., Flores-Herrera, O., & Zazueta, C. (2019). The relevance of the supramolecular arrangements of the respiratory chain complexes in human diseases and aging. *Mitochondrion*. <https://doi.org/10.1016/J.MITO.2019.01.001>

Rangarajan, P., Karthikeyan, A., Lu, J., Ling, E. A., & Dheen, S. T. (2015). Sirtuin 3 regulates Foxo3a-mediated antioxidant pathway in microglia. *Neuroscience*, 311, 398–414.

<https://doi.org/10.1016/j.neuroscience.2015.10.048>

Ray, P. D., Huang, B.-W., & Tsuji, Y. (2012). Reactive oxygen species (ROS) homeostasis and redox regulation in cellular signaling. *Cellular Signalling*, 24, 981–990.

<https://doi.org/10.1016/j.cellsig.2012.01.008>

Ruetenik, A., & Barrientos, A. (2015). Dietary restriction, mitochondrial function and aging: From yeast to humans. *Biochimica et Biophysica Acta - Bioenergetics*, 1847(11), 1434–1447.

<https://doi.org/10.1016/j.bbabi.2015.05.005>

Sena, L. A., & Chandel, N. S. (2012). Molecular Cell Review Physiological Roles of Mitochondrial Reactive Oxygen Species. *Molecular Cell*, 48, 158–167.

<https://doi.org/10.1016/j.molcel.2012.09.025>

Sgarbi, G., Matarrese, P., Pinti, M., Lanzarini, C., Ascione, B., Gibellini, L., ... Salvioli, S. (2014). Mitochondria hyperfusion and elevated autophagic activity are key mechanisms for cellular bioenergetic preservation in centenarians. *Aging*, 6(4), 296–310. Retrieved from www.impactaging.com

Sheng, B., Wang, X., Su, B., Lee, H., Casadesus, G., Perry, G., & Zhu, X. (2012). Impaired mitochondrial biogenesis contributes to mitochondrial dysfunction in Alzheimer's disease. *Journal of Neurochemistry*, 120(3), 419–429. <https://doi.org/10.1111/j.1471-4159.2011.07581.x>

Starkov, A. A., & Fiskum, G. (2003). Regulation of brain mitochondrial H₂O₂ production by membrane potential and NAD(P)H redox state. *Journal of Neurochemistry*, 86(5), 1101–1107.

<https://doi.org/10.1046/j.1471-4159.2003.01908.x>

Stein, L. R., & Imai, S. I. (2012). The dynamic regulation of NAD metabolism in mitochondria. *Trends in Endocrinology and Metabolism*, 23(9), 420–428.

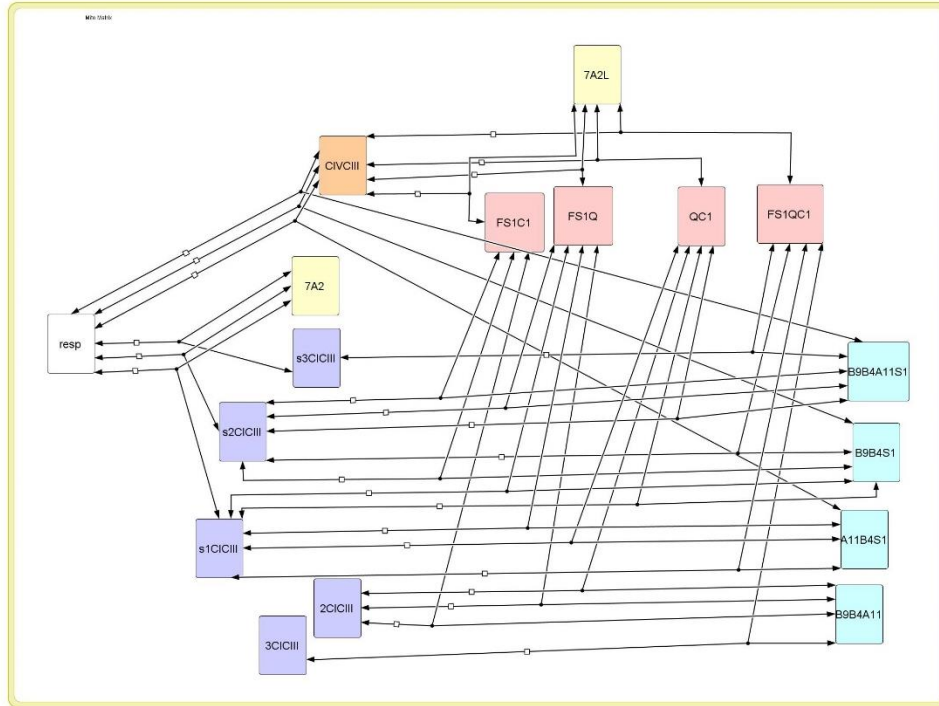
<https://doi.org/10.1016/j.tem.2012.06.005>

Stroud, D. A., Surgenor, E. E., Formosa, L. E., Reljic, B., Frazier, A. E., Dibley, M. G., ... Ryan, M. T. (2016). Accessory subunits are integral for assembly and function of human mitochondrial complex I. *Nature*, 538, 123–126. Retrieved from <https://core.ac.uk/download/pdf/153544165.pdf>

Sun, Y., Oberley, L. W., & Li, Y. (1988). A simple method for clinical assay of superoxide dismutase. *Clinical Chemistry*, 34(3), 497–500. <https://doi.org/10.1074/jbc.M113.471342>

- Swerdlow, R. H., Burns, J. M., & Khan, S. M. (2010). The Alzheimer's disease mitochondrial cascade hypothesis. *Journal of Alzheimer's Disease: JAD*, *20*(Suppl 2), S265-79. <https://doi.org/10.3233/JAD-2010-100339>
- The Uniprot Consortium. (2019). UniProt: a worldwide hub of protein knowledge. *Nucleic Acids Research*, *47*(D1), D506–D515. <https://doi.org/10.1093/nar/gky1049>
- Wang, M., Herrmann, C. J., Simonovic, M., Szklarczyk, D., & von Mering, C. (2015). Version 4.0 of PaxDb: Protein abundance data, integrated across model organisms, tissues, and cell-lines. *PROTEOMICS*, *15*(18), 3163–3168. <https://doi.org/10.1002/pmic.201400441>
- Wishart, D. S., Feunang, Y. D., Marcu, A., Guo, A. C., Liang, K., Vázquez-Fresno, R., ... Scalbert, A. (2018). HMDB 4.0: the human metabolome database for 2018. *Nucleic Acids Research*, *46*(D1), D608–D617. <https://doi.org/10.1093/nar/gkx1089>
- Xie, Y., Allaire, J. J., & Grolemond, G. (2019). *R Markdown: The Definitive Guide*. Chapman & Hall/CRC. Retrieved from <https://bookdown.org/yihui/rmarkdown/>
- Yu, W., Dittenhafer-Reed, K. E., & Denu, J. M. (2012). SIRT3 protein deacetylates isocitrate dehydrogenase 2 (IDH2) and regulates mitochondrial redox status. *The Journal of Biological Chemistry*, *287*(17), 14078–14086. <https://doi.org/10.1074/jbc.M112.355206>
- Zhang, M., Deng, Y.-N., Zhang, J.-Y., Liu, J., Li, Y.-B., Su, H., & Qu, Q.-M. (2018). SIRT3 Protects Rotenone-induced Injury in SH-SY5Y Cells by Promoting Autophagy through the LKB1-AMPK-mTOR Pathway. *Aging and Disease*, *9*(2), 273. <https://doi.org/10.14336/AD.2017.0517>
- Zrelli, H., Matsuoka, M., Kitazaki, S., Zarrouk, M., & Miyazaki, H. (2011). Hydroxytyrosol reduces intracellular reactive oxygen species levels in vascular endothelial cells by upregulating catalase expression through the AMPK-FOXO3a pathway. *European Journal of Pharmacology*, *660*(2–3), 275–282. <https://doi.org/10.1016/j.ejphar.2011.03.045>

S1: Complete SC model

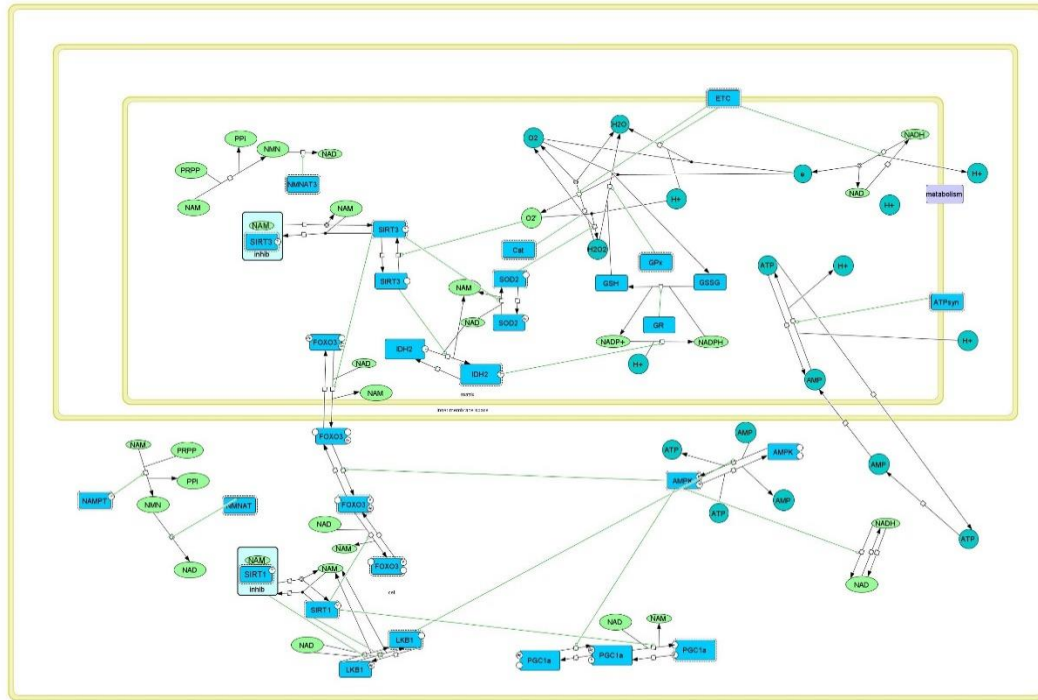


S1: Model of potential SC assemblies based on Subunit expression. CI is shown in light blue, CIII in red and CIV in purple. SC C1CIII is shown in purple, CIVCIII in orange and Respirasome in white. The letter and number pairs represent the potential groupings of subunits (CI(blue): B9=NDUFB9, B4=NDUFB4, A11=NDUFA11 and S1=NDUFS1; CIII(red): FS1=UQCRFS1, Q=UQCRQ, and C1=UQCRC1; CIV(orange): 7AL=COX7AL, and 7A2=COX7A2). C1CIII is differentiated by the number of stable inter-complex bonds being formed with 3 being the most in 1 the least. The prefix "s" represents the presence of CI subunit NDUFS1, an essential subunit for respirasome formation. This models represents all potential combinations.

$$\begin{aligned}
 \frac{d([B9B4A11S1] \cdot V_{\text{Mito Matrix}})}{dt} &= -V_{\text{Mito Matrix}} \left(\frac{kf_re650_{(re650)} [B9B4A11S1] \cdot V_{\text{Mito Matrix}} \cdot [CIVCIII] \cdot V_{\text{Mito Matrix}} - kr_re650_{(re650)} [resp] \cdot V_{\text{Mito Matrix}}}{V_{\text{Mito Matrix}}} \right) \\
 &\quad - V_{\text{Mito Matrix}} \left(\frac{kf_re657_{(re657)} [B9B4A11S1] \cdot V_{\text{Mito Matrix}} \cdot [FS1QR11C1] \cdot V_{\text{Mito Matrix}} - kr_re657_{(re657)} [s3CICIII] \cdot V_{\text{Mito Matrix}}}{V_{\text{Mito Matrix}}} \right) \\
 &\quad - V_{\text{Mito Matrix}} \left(\frac{kf_re661_{(re661)} [B9B4A11S1] \cdot V_{\text{Mito Matrix}} \cdot [FS1R11C1] \cdot V_{\text{Mito Matrix}} - kr_re661_{(re661)} [s2CICIII] \cdot V_{\text{Mito Matrix}}}{V_{\text{Mito Matrix}}} \right) \\
 \frac{d([B9B4S1] \cdot V_{\text{Mito Matrix}})}{dt} &= -V_{\text{Mito Matrix}} \left(\frac{kf_re649_{(re649)} [B9B4S1] \cdot V_{\text{Mito Matrix}} \cdot [CIVCIII] \cdot V_{\text{Mito Matrix}} - kr_re649_{(re649)} [resp] \cdot V_{\text{Mito Matrix}}}{V_{\text{Mito Matrix}}} \right) \\
 &\quad - V_{\text{Mito Matrix}} \left(\frac{kf_re652_{(re652)} [B9B4S1] \cdot V_{\text{Mito Matrix}} \cdot [FS1QR11C1] \cdot V_{\text{Mito Matrix}} - kr_re652_{(re652)} [s2CICIII] \cdot V_{\text{Mito Matrix}}}{V_{\text{Mito Matrix}}} \right) \\
 &\quad - V_{\text{Mito Matrix}} \left(\frac{kf_re654_{(re654)} [B9B4S1] \cdot V_{\text{Mito Matrix}} \cdot [FS1R11C1] \cdot V_{\text{Mito Matrix}} - kr_re654_{(re654)} [s2CICIII] \cdot V_{\text{Mito Matrix}}}{V_{\text{Mito Matrix}}} \right) \\
 \frac{d([FS1QR11C1] \cdot V_{\text{Mito Matrix}})}{dt} &= -V_{\text{Mito Matrix}} \left(\frac{kf_re652_{(re652)} [B9B4S1] \cdot V_{\text{Mito Matrix}} \cdot [FS1QR11C1] \cdot V_{\text{Mito Matrix}} - kr_re652_{(re652)} [s2CICIII] \cdot V_{\text{Mito Matrix}}}{V_{\text{Mito Matrix}}} \right) \\
 &\quad - V_{\text{Mito Matrix}} \left(\frac{kf_re657_{(re657)} [B9B4A11S1] \cdot V_{\text{Mito Matrix}} \cdot [FS1QR11C1] \cdot V_{\text{Mito Matrix}} - kr_re657_{(re657)} [s3CICIII] \cdot V_{\text{Mito Matrix}}}{V_{\text{Mito Matrix}}} \right) \\
 &\quad - V_{\text{Mito Matrix}} \left(\frac{kf_re690_{(re690)} [FS1QR11C1] \cdot V_{\text{Mito Matrix}} \cdot [7A2L] \cdot V_{\text{Mito Matrix}} - kr_re690_{(re690)} [CIVCIII] \cdot V_{\text{Mito Matrix}}}{V_{\text{Mito Matrix}}} \right) \\
 \frac{d([7A2L] \cdot V_{\text{Mito Matrix}})}{dt} &= -V_{\text{Mito Matrix}} \left(\frac{kf_re690_{(re690)} [FS1QR11C1] \cdot V_{\text{Mito Matrix}} \cdot [7A2L] \cdot V_{\text{Mito Matrix}} - kr_re690_{(re690)} [CIVCIII] \cdot V_{\text{Mito Matrix}}}{V_{\text{Mito Matrix}}} \right) \\
 &\quad - V_{\text{Mito Matrix}} \left(\frac{kf_re693_{(re693)} [7A2L] \cdot V_{\text{Mito Matrix}} \cdot [FS1R11C1] \cdot V_{\text{Mito Matrix}} - kr_re693_{(re693)} [CIVCIII] \cdot V_{\text{Mito Matrix}}}{V_{\text{Mito Matrix}}} \right) \\
 \\
 \frac{d([7A2] \cdot V_{\text{Mito Matrix}})}{dt} &= -V_{\text{Mito Matrix}} \cdot ((k1_{(re647)} [7A2] \cdot [s3CICIII] - k2_{(re647)} [resp])) \\
 &\quad - V_{\text{Mito Matrix}} \left(\frac{kf_re648_{(re648)} [s2CICIII] \cdot V_{\text{Mito Matrix}} \cdot [7A2] \cdot V_{\text{Mito Matrix}} - kr_re648_{(re648)} [resp] \cdot V_{\text{Mito Matrix}}}{V_{\text{Mito Matrix}}} \right) \\
 &\quad - V_{\text{Mito Matrix}} \left(\frac{kf_re666_{(re666)} [s1CICIII] \cdot V_{\text{Mito Matrix}} \cdot [7A2] \cdot V_{\text{Mito Matrix}} - kr_re666_{(re666)} [resp] \cdot V_{\text{Mito Matrix}}}{V_{\text{Mito Matrix}}} \right) \\
 \frac{d([CIVCIII] \cdot V_{\text{Mito Matrix}})}{dt} &= -V_{\text{Mito Matrix}} \left(\frac{kf_re649_{(re649)} [B9B4S1] \cdot V_{\text{Mito Matrix}} \cdot [CIVCIII] \cdot V_{\text{Mito Matrix}} - kr_re649_{(re649)} [resp] \cdot V_{\text{Mito Matrix}}}{V_{\text{Mito Matrix}}} \right) \\
 &\quad - V_{\text{Mito Matrix}} \left(\frac{kf_re650_{(re650)} [B9B4A11S1] \cdot V_{\text{Mito Matrix}} \cdot [CIVCIII] \cdot V_{\text{Mito Matrix}} - kr_re650_{(re650)} [resp] \cdot V_{\text{Mito Matrix}}}{V_{\text{Mito Matrix}}} \right) \\
 &\quad + V_{\text{Mito Matrix}} \left(\frac{kf_re690_{(re690)} [FS1QR11C1] \cdot V_{\text{Mito Matrix}} \cdot [7A2L] \cdot V_{\text{Mito Matrix}} - kr_re690_{(re690)} [CIVCIII] \cdot V_{\text{Mito Matrix}}}{V_{\text{Mito Matrix}}} \right) \\
 &\quad + V_{\text{Mito Matrix}} \left(\frac{kf_re693_{(re693)} [7A2L] \cdot V_{\text{Mito Matrix}} \cdot [FS1R11C1] \cdot V_{\text{Mito Matrix}} - kr_re693_{(re693)} [CIVCIII] \cdot V_{\text{Mito Matrix}}}{V_{\text{Mito Matrix}}} \right) \\
 \frac{d([s3CICIII] \cdot V_{\text{Mito Matrix}})}{dt} &= -V_{\text{Mito Matrix}} \cdot ((k1_{(re647)} [7A2] \cdot [s3CICIII] - k2_{(re647)} [resp])) \\
 &\quad + V_{\text{Mito Matrix}} \left(\frac{kf_re657_{(re657)} [B9B4A11S1] \cdot V_{\text{Mito Matrix}} \cdot [FS1QR11C1] \cdot V_{\text{Mito Matrix}} - kr_re657_{(re657)} [s3CICIII] \cdot V_{\text{Mito Matrix}}}{V_{\text{Mito Matrix}}} \right)
 \end{aligned}$$

$$\begin{aligned}
 \frac{d([s2CICIII] \cdot V_{\text{Mito Matrix}})}{dt} &= -V_{\text{Mito Matrix}} \left(\frac{kf_re648_{(re648)} \cdot [s2CICIII] \cdot V_{\text{Mito Matrix}} \cdot [7A2] \cdot V_{\text{Mito Matrix}} - kr_re648_{(re648)} \cdot [resp] \cdot V_{\text{Mito Matrix}}}{V_{\text{Mito Matrix}}} \right) \\
 &+ V_{\text{Mito Matrix}} \left(\frac{kf_re652_{(re652)} \cdot [B9B4S1] \cdot V_{\text{Mito Matrix}} \cdot [FS1QR11C1] \cdot V_{\text{Mito Matrix}} - kr_re652_{(re652)} \cdot [s2CICIII] \cdot V_{\text{Mito Matrix}}}{V_{\text{Mito Matrix}}} \right) \\
 &+ V_{\text{Mito Matrix}} \left(\frac{kf_re654_{(re654)} \cdot [B9B4S1] \cdot V_{\text{Mito Matrix}} \cdot [FS1R11C1] \cdot V_{\text{Mito Matrix}} - kr_re654_{(re654)} \cdot [s2CICIII] \cdot V_{\text{Mito Matrix}}}{V_{\text{Mito Matrix}}} \right) \\
 &+ V_{\text{Mito Matrix}} \left(\frac{kf_re661_{(re661)} \cdot [B9B4A11S1] \cdot V_{\text{Mito Matrix}} \cdot [FS1R11C1] \cdot V_{\text{Mito Matrix}} - kr_re661_{(re661)} \cdot [s2CICIII] \cdot V_{\text{Mito Matrix}}}{V_{\text{Mito Matrix}}} \right) \\
 \frac{d([s1CICIII] \cdot V_{\text{Mito Matrix}})}{dt} &= -V_{\text{Mito Matrix}} \left(\frac{kf_re666_{(re666)} \cdot [s1CICIII] \cdot V_{\text{Mito Matrix}} \cdot [7A2] \cdot V_{\text{Mito Matrix}} - kr_re666_{(re666)} \cdot [resp] \cdot V_{\text{Mito Matrix}}}{V_{\text{Mito Matrix}}} \right) \\
 \frac{d([resp] \cdot V_{\text{Mito Matrix}})}{dt} &= +V_{\text{Mito Matrix}} \cdot ((k1_{(re647)} \cdot [7A2] \cdot [s3CICIII] - k2_{(re647)} \cdot [resp])) \\
 &+ V_{\text{Mito Matrix}} \left(\frac{kf_re648_{(re648)} \cdot [s2CICIII] \cdot V_{\text{Mito Matrix}} \cdot [7A2] \cdot V_{\text{Mito Matrix}} - kr_re648_{(re648)} \cdot [resp] \cdot V_{\text{Mito Matrix}}}{V_{\text{Mito Matrix}}} \right) \\
 &+ V_{\text{Mito Matrix}} \left(\frac{kf_re649_{(re649)} \cdot [B9B4S1] \cdot V_{\text{Mito Matrix}} \cdot [CIVCIII] \cdot V_{\text{Mito Matrix}} - kr_re649_{(re649)} \cdot [resp] \cdot V_{\text{Mito Matrix}}}{V_{\text{Mito Matrix}}} \right) \\
 &+ V_{\text{Mito Matrix}} \left(\frac{kf_re650_{(re650)} \cdot [B9B4A11S1] \cdot V_{\text{Mito Matrix}} \cdot [CIVCIII] \cdot V_{\text{Mito Matrix}} - kr_re650_{(re650)} \cdot [resp] \cdot V_{\text{Mito Matrix}}}{V_{\text{Mito Matrix}}} \right) \\
 &+ V_{\text{Mito Matrix}} \left(\frac{kf_re666_{(re666)} \cdot [s1CICIII] \cdot V_{\text{Mito Matrix}} \cdot [7A2] \cdot V_{\text{Mito Matrix}} - kr_re666_{(re666)} \cdot [resp] \cdot V_{\text{Mito Matrix}}}{V_{\text{Mito Matrix}}} \right) \\
 \\
 \frac{d([FS1R11C1] \cdot V_{\text{Mito Matrix}})}{dt} &= -V_{\text{Mito Matrix}} \left(\frac{kf_re654_{(re654)} \cdot [B9B4S1] \cdot V_{\text{Mito Matrix}} \cdot [FS1R11C1] \cdot V_{\text{Mito Matrix}} - kr_re654_{(re654)} \cdot [s2CICIII] \cdot V_{\text{Mito Matrix}}}{V_{\text{Mito Matrix}}} \right) \\
 &- V_{\text{Mito Matrix}} \left(\frac{kf_re661_{(re661)} \cdot [B9B4A11S1] \cdot V_{\text{Mito Matrix}} \cdot [FS1R11C1] \cdot V_{\text{Mito Matrix}} - kr_re661_{(re661)} \cdot [s2CICIII] \cdot V_{\text{Mito Matrix}}}{V_{\text{Mito Matrix}}} \right) \\
 &- V_{\text{Mito Matrix}} \left(\frac{kf_re693_{(re693)} \cdot [7A2] \cdot V_{\text{Mito Matrix}} \cdot [FS1R11C1] \cdot V_{\text{Mito Matrix}} - kr_re693_{(re693)} \cdot [CIVCIII] \cdot V_{\text{Mito Matrix}}}{V_{\text{Mito Matrix}}} \right) \\
 [tCI] &= [2CICIII] + [3CICIII] + [B9B4A11S1] + [B9B4S1] + [resp] + [s1CICIII] + [s2CICIII] + [s3CICIII] \\
 \%CIII &= \frac{100 \cdot ([FS1QR11C1] + [FS1R11C1])}{[FS1QR11C1] + [FS1R11C1] + [resp] + [s1CICIII] + [s2CICIII] + [s3CICIII] + [2CICIII] + [3CICIII]} \\
 [CIV] &= \%CIV \\
 \%resp &= \frac{100 \cdot [resp]}{[tCI]} \\
 \\
 [CI] &= \frac{100 \cdot ([B9B4A11S1] + [B9B4S1])}{[tCI]} \\
 \%CICIII &= \frac{100 \cdot ([2CICIII] + [3CICIII] + [s1CICIII] + [s2CICIII] + [s3CICIII])}{[tCI]} \\
 \%CIV &= \frac{tCIV}{tCIV + [CIVCIII] + [resp]} \\
 tCIV &= [COX7A2] + [COX7A2L] \\
 \%CI &= \frac{100 \cdot ([B9B4A11S1] + [B9B4S1])}{[tCI]} \\
 \%resp &= \frac{100 \cdot [resp]}{[tCI]} \\
 \%CICIII &= \frac{100 \cdot ([2CICIII] + [3CICIII] + [s1CICIII] + [s2CICIII] + [s3CICIII])}{[tCI]}
 \end{aligned}$$

re647		$\mu\text{mol}/(\text{l}^*\text{s})$
	k1	$0.5 \text{ l}/(\mu\text{mol}^*\text{s})$
	k2	0.05 1/s
re648		$\mu\text{mol}/(\text{l}^*\text{s})$
	kf_re648	$0.3 \text{ 1}/(\mu\text{mol}^*\text{s})$
	kr_re648	0.05 1/s
re649		$\mu\text{mol}/(\text{l}^*\text{s})$
	kf_re649	$0.7 \text{ 1}/(\mu\text{mol}^*\text{s})$
	kr_re649	0.05 1/s
re650		$\mu\text{mol}/(\text{l}^*\text{s})$
	kf_re650	$0.7 \text{ 1}/(\mu\text{mol}^*\text{s})$
	kr_re650	0.05 1/s
re652		$\mu\text{mol}/(\text{l}^*\text{s})$
	kf_re652	$0.8 \text{ 1}/(\mu\text{mol}^*\text{s})$
	kr_re652	0.05 1/s
re654		$\mu\text{mol}/(\text{l}^*\text{s})$
	kf_re654	$0.8 \text{ 1}/(\mu\text{mol}^*\text{s})$
	kr_re654	0.05 1/s
re657		$\mu\text{mol}/(\text{l}^*\text{s})$
	kf_re657	$0.9 \text{ 1}/(\mu\text{mol}^*\text{s})$
	kr_re657	0.01 1/s
re661		$\text{nan } \mu\text{mol}/(\text{l}^*\text{s})$
	kf_re661	$0.8 \text{ 1}/(\mu\text{mol}^*\text{s})$
	kr_re661	0.05 1/s
re666		$\text{nan } \mu\text{mol}/(\text{l}^*\text{s})$
	kf_re666	$0.3 \text{ 1}/(\mu\text{mol}^*\text{s})$
	kr_re666	0.01 1/s
re690		$\text{nan } \mu\text{mol}/(\text{l}^*\text{s})$
	kf_re690	$0.3 \text{ 1}/(\mu\text{mol}^*\text{s})$
	kr_re690	0.05 1/s
re693		$\text{nan } \mu\text{mol}/(\text{l}^*\text{s})$
	kf_re693	$0.3 \text{ 1}/(\mu\text{mol}^*\text{s})$
	kr_re693	0.05 1/s



S3: Oxidative stress model showing each explicit reaction used to create the differential equation system.

Modeling the effects of SC formation and stress response on AD progression
 S4: Oxidative Stress Model Equations

$$\begin{aligned}
 \frac{d([\text{SOD2}]:V_{\text{matrix}})}{dt} &= -V_{\text{matrix}} \left(\frac{k_{\text{cat_re13_s85}}}{k_{\text{ic_re13_s22_s85}} + k_{\text{m_re13_s4_s85}} + [\text{SOD2}]:[\text{NAD}(\text{matrix})] + k_{\text{m_re13_s4_s85}} + [\text{SOD2}] + k_{\text{m_re13_s22_s85}}} \right) [\text{aSIRT3}]:[\text{NAD}(\text{matrix})]:[\text{SOD2}] \\
 &+ V_{\text{matrix}} \left(k_1 [\text{SOD2}]:\text{deact} \right) [\text{aSOD2}] \\
 \frac{d([\text{NADH}(\text{matrix})]:V_{\text{matrix}})}{dt} &= +V_{\text{matrix}} \left([\text{metabolic}] \left(\frac{k_{\text{cat_re40_s105}}}{k_{\text{m_re40_s102_s105}}} [\text{NAD}(\text{matrix})] \right) \right) \\
 &- \left(V_{\text{matrix}} \left(\frac{k_{\text{cat_re7_s21}}}{k_{\text{m_re7_s16_s21}}} [\text{NADH}(\text{matrix})] \right) \right) \\
 &+ V_{\text{matrix}} \left([\text{ETC}] \left(\frac{k_{\text{cat_re7_s21}}}{k_{\text{m_re7_s16_s21}}} [\text{NADH}(\text{matrix})] \right) \right) \\
 \frac{d([\text{aSOD2}]:V_{\text{matrix}})}{dt} &= +V_{\text{matrix}} \left(\frac{k_{\text{cat_re13_s85}}}{k_{\text{ic_re13_s22_s85}} + k_{\text{m_re13_s4_s85}} + [\text{SOD2}]:[\text{NAD}(\text{matrix})] + k_{\text{m_re13_s4_s85}} + [\text{SOD2}] + k_{\text{m_re13_s22_s85}}} \right) [\text{aSIRT3}]:[\text{NAD}(\text{matrix})]:[\text{SOD2}] \\
 &- V_{\text{matrix}} \left(k_1 [\text{SOD2}]:\text{deact} \right) [\text{aSOD2}] \\
 \frac{d([\text{ATP}(\text{matrix})]:V_{\text{matrix}})}{dt} &= -V_{\text{matrix}} \left(k_{\text{f_re7}} [\text{ATP}(\text{matrix})] \right) \\
 &+ \left(\frac{V_{\text{inner membrane space}} \cdot k_{\text{cat_re14_s83}}}{k_{\text{ic_re14_s20_s83}} + k_{\text{m_re14_s90_s83}} + [\text{AMP}(\text{matrix})]:[\text{H}+(\text{inner membrane space})]} \right) [\text{ATPsyn}]:[\text{H}+(\text{inner membrane space})]:[\text{AMP}(\text{matrix})] \\
 &- V_{\text{matrix}} \left(k_1 [\text{ATP}(\text{matrix})]:\text{deact} \right) [\text{ATP}(\text{matrix})] \\
 \frac{d([\text{GSSG}]:V_{\text{matrix}})}{dt} &= +V_{\text{matrix}} \left(\frac{k_{\text{cat_re11_s63}}}{k_{\text{ic_re11_s18_s63}} + k_{\text{m_re11_s60_s63}} + [\text{H2O2}]:[\text{GSH}] + k_{\text{m_re11_s60_s63}} + [\text{H2O2}]:[\text{GSH}] + k_{\text{m_re11_s18_s63}}} \right) [\text{GPx}]:[\text{GSH}]:[\text{H2O2}] \\
 &- V_{\text{matrix}} \left(\frac{k_{\text{cat_re18_s64}}}{k_{\text{ic_re18_s59_s64}} + k_{\text{m_re18_s62_s64}} + [\text{GSSG}]:[\text{NADPH}] + k_{\text{m_re18_s62_s64}} + [\text{GSSG}]:[\text{NADPH}] + k_{\text{m_re18_s59_s64}}} \right) [\text{GPx}]:[\text{GSH}]:[\text{H2O2}] \\
 &+ V_{\text{matrix}} \left(\frac{k_{\text{cat_re18_s64}}}{k_{\text{ic_re18_s59_s64}} + k_{\text{m_re18_s62_s64}} + [\text{GSSG}]:[\text{NADPH}] + k_{\text{m_re18_s62_s64}} + [\text{GSSG}]:[\text{NADPH}] + k_{\text{m_re18_s59_s64}}} \right) [\text{GPx}]:[\text{GSH}]:[\text{H2O2}] \\
 \frac{d([\text{GSH}]:V_{\text{matrix}})}{dt} &= -V_{\text{matrix}} \left(\frac{k_{\text{cat_re11_s63}}}{k_{\text{ic_re11_s18_s63}} + k_{\text{m_re11_s60_s63}} + [\text{H2O2}]:[\text{GSH}] + k_{\text{m_re11_s60_s63}} + [\text{H2O2}]:[\text{GSH}] + k_{\text{m_re11_s18_s63}}} \right) [\text{GPx}]:[\text{GSH}]:[\text{H2O2}] \\
 &+ V_{\text{matrix}} \left(\frac{k_{\text{cat_re18_s64}}}{k_{\text{ic_re18_s59_s64}} + k_{\text{m_re18_s62_s64}} + [\text{GSSG}]:[\text{NADPH}] + k_{\text{m_re18_s62_s64}} + [\text{GSSG}]:[\text{NADPH}] + k_{\text{m_re18_s59_s64}}} \right) [\text{GPx}]:[\text{GSH}]:[\text{H2O2}] \\
 &+ V_{\text{matrix}} \left(\frac{k_{\text{cat_re18_s64}}}{k_{\text{ic_re18_s59_s64}} + k_{\text{m_re18_s62_s64}} + [\text{GSSG}]:[\text{NADPH}] + k_{\text{m_re18_s62_s64}} + [\text{GSSG}]:[\text{NADPH}] + k_{\text{m_re18_s59_s64}}} \right) [\text{GPx}]:[\text{GSH}]:[\text{H2O2}] \\
 \frac{d([\text{NADP}^+]:V_{\text{matrix}})}{dt} &= +V_{\text{matrix}} \left(\frac{k_{\text{cat_re18_s64}}}{k_{\text{ic_re18_s59_s64}} + k_{\text{m_re18_s62_s64}} + [\text{GSSG}]:[\text{NADPH}] + k_{\text{m_re18_s62_s64}} + [\text{GSSG}]:[\text{NADPH}] + k_{\text{m_re18_s59_s64}}} \right) [\text{GPx}]:[\text{GSH}]:[\text{H2O2}] \\
 &- V_{\text{matrix}} \left(\frac{k_{\text{cat_re73_s127}}}{k_{\text{ic_re73_s61_s127}} + k_{\text{m_re73_s6_s127}} + [\text{NADP}^+]:[\text{H}+(\text{matrix})]} \right) [\text{aIDH2}]:[\text{H}+(\text{matrix})]:[\text{NADP}^+] \\
 &+ V_{\text{matrix}} \left(\frac{k_{\text{cat_re18_s64}}}{k_{\text{ic_re18_s59_s64}} + k_{\text{m_re18_s62_s64}} + [\text{GSSG}]:[\text{NADPH}] + k_{\text{m_re18_s62_s64}} + [\text{GSSG}]:[\text{NADPH}] + k_{\text{m_re18_s59_s64}}} \right) [\text{GPx}]:[\text{GSH}]:[\text{H2O2}] \\
 \frac{d([\text{NADPH}]:V_{\text{matrix}})}{dt} &= -V_{\text{matrix}} \left(\frac{k_{\text{cat_re18_s64}}}{k_{\text{ic_re18_s59_s64}} + k_{\text{m_re18_s62_s64}} + [\text{GSSG}]:[\text{NADPH}] + k_{\text{m_re18_s62_s64}} + [\text{GSSG}]:[\text{NADPH}] + k_{\text{m_re18_s59_s64}}} \right) [\text{GPx}]:[\text{GSH}]:[\text{H2O2}] \\
 &+ V_{\text{matrix}} \left(\frac{k_{\text{cat_re73_s127}}}{k_{\text{ic_re73_s61_s127}} + k_{\text{m_re73_s6_s127}} + [\text{NADP}^+]:[\text{H}+(\text{matrix})]} \right) [\text{aIDH2}]:[\text{H}+(\text{matrix})]:[\text{NADP}^+] \\
 &+ V_{\text{matrix}} \left(\frac{k_{\text{cat_re18_s64}}}{k_{\text{ic_re18_s59_s64}} + k_{\text{m_re18_s62_s64}} + [\text{GSSG}]:[\text{NADPH}] + k_{\text{m_re18_s62_s64}} + [\text{GSSG}]:[\text{NADPH}] + k_{\text{m_re18_s59_s64}}} \right) [\text{GPx}]:[\text{GSH}]:[\text{H2O2}] \\
 \frac{d([\text{LKB1}]:V_{\text{cell}})}{dt} &= -V_{\text{cell}} \left(\frac{k_{\text{cat_re37_s69_s88}}}{k_{\text{ic_re37_s69_s88}} + k_{\text{m_re37_s114_s88}} + [\text{LKB1}]:[\text{NAD}(\text{cell})]} \right) [\text{SIRT1}]:[\text{NAD}(\text{cell})]:[\text{LKB1}] \\
 &+ V_{\text{cell}} \left(k_1 [\text{LKB1}]:\text{deact} \right) [\text{LKB1}] \\
 \frac{d([\text{LKB1}]:V_{\text{cell}})}{dt} &= -V_{\text{cell}} \left(\frac{k_{\text{cat_re37_s69_s88}}}{k_{\text{ic_re37_s69_s88}} + k_{\text{m_re37_s114_s88}} + [\text{LKB1}]:[\text{NAD}(\text{cell})]} \right) [\text{SIRT1}]:[\text{NAD}(\text{cell})]:[\text{LKB1}] \\
 &+ V_{\text{cell}} \left(k_1 [\text{LKB1}]:\text{deact} \right) [\text{LKB1}] \\
 \frac{d([\text{AMPK}]:V_{\text{cell}})}{dt} &= -V_{\text{cell}} \left(\frac{k_{\text{cat_re20_s70}}}{k_{\text{ic_re20_s29_s70}} + k_{\text{m_re20_s116_s70}} + [\text{AMPK}]:[\text{AMP}(\text{cell})]} \right) [\text{aLKB1}]:[\text{AMP}(\text{cell})]:[\text{AMPK}] \\
 &+ V_{\text{cell}} \left(\frac{V_{\text{matrix}} \cdot k_{\text{f_re21}}}{V_{\text{cell}}} \right) [\text{AMPK}]:[\text{ATP}(\text{cell})] \\
 \frac{d([\text{PRPP}(\text{matrix})]:V_{\text{matrix}})}{dt} &= -V_{\text{matrix}} \left(k_1 [\text{NAM}(\text{matrix})]:\text{deact} \right) [\text{NAM}(\text{matrix})]:[\text{PRPP}(\text{matrix})] \\
 &+ V_{\text{matrix}} \left(k_1 [\text{NAM}(\text{matrix})]:\text{deact} \right) [\text{NAM}(\text{matrix})]:[\text{PRPP}(\text{matrix})] \\
 \frac{d([\text{NMN}(\text{matrix})]:V_{\text{matrix}})}{dt} &= -V_{\text{matrix}} \left(\frac{k_{\text{cat_re27_s51}}}{k_{\text{ic_re27_s47_s51}} + k_{\text{m_re27_s47_s51}}} \right) [\text{NAM}(\text{matrix})]:[\text{PRPP}(\text{matrix})] \\
 &+ V_{\text{matrix}} \left(k_1 [\text{NAM}(\text{matrix})]:\text{deact} \right) [\text{NAM}(\text{matrix})]:[\text{PRPP}(\text{matrix})] \\
 \frac{d([\text{NAD}(\text{matrix})]:V_{\text{matrix}})}{dt} &= -V_{\text{matrix}} \left([\text{metabolic}] \left(\frac{k_{\text{cat_re40_s105}}}{k_{\text{m_re40_s102_s105}}} [\text{NAD}(\text{matrix})] \right) \right) \\
 &+ \left(V_{\text{matrix}} \left(\frac{k_{\text{cat_re7_s21}}}{k_{\text{m_re7_s16_s21}}} [\text{NADH}(\text{matrix})] \right) \right) \\
 &+ V_{\text{matrix}} \left([\text{ETC}] \left(\frac{k_{\text{cat_re7_s21}}}{k_{\text{m_re7_s16_s21}}} [\text{NADH}(\text{matrix})] \right) \right) \\
 &+ V_{\text{matrix}} \left([\text{NMNAT3}] \left(\frac{k_{\text{cat_re27_s51}}}{k_{\text{m_re27_s47_s51}}} [\text{NAM}(\text{matrix})] \right) \right) \\
 &- V_{\text{matrix}} \left(\frac{k_{\text{cat_re13_s85}}}{k_{\text{ic_re13_s22_s85}} + k_{\text{m_re13_s4_s85}} + [\text{SOD2}]:[\text{NAD}(\text{matrix})] + k_{\text{m_re13_s4_s85}} + [\text{SOD2}] + k_{\text{m_re13_s22_s85}}} \right) [\text{aSIRT3}]:[\text{NAD}(\text{matrix})]:[\text{SOD2}] \\
 &- V_{\text{matrix}} \left(\frac{k_{\text{cat_re24_s85}}}{k_{\text{ic_re24_s81_s85}} + k_{\text{m_re24_s4_s85}} + [\text{FOXO3}]:[\text{NAD}(\text{matrix})] + k_{\text{m_re24_s4_s85}} + [\text{FOXO3}]:[\text{NAD}(\text{matrix})] + k_{\text{m_re24_s81_s85}}} \right) [\text{aSIRT3}]:[\text{NAD}(\text{matrix})]:[\text{FOXO3}] \\
 &- V_{\text{matrix}} \left(\frac{k_{\text{cat_re86_s5}}}{k_{\text{ic_re86_s127_s5}} + k_{\text{m_re86_s4_s5}} + [\text{IDH2}]:[\text{NAD}(\text{matrix})] + k_{\text{m_re86_s4_s5}} + [\text{IDH2}]:[\text{NAD}(\text{matrix})] + k_{\text{m_re86_s127_s5}}} \right) [\text{aSIRT3}]:[\text{NAD}(\text{matrix})]:[\text{IDH2}] \\
 \frac{d([\text{SIRT3}]:V_{\text{matrix}})}{dt} &= +V_{\text{matrix}} \left(k_1 [\text{SIRT3}]:\text{deact} \right) [\text{aSIRT3}] \\
 &- V_{\text{matrix}} \left(\frac{k_{\text{cat_re14_s83}}}{k_{\text{ic_re14_s20_s83}} + k_{\text{m_re14_s90_s83}} + [\text{AMP}(\text{matrix})]:[\text{H}+(\text{inner membrane space})]} \right) [\text{ATPsyn}]:[\text{H}+(\text{inner membrane space})]:[\text{AMP}(\text{matrix})] \\
 &- V_{\text{matrix}} \left([\text{O2}^{\cdot -}] \left(\frac{k_{\text{cat_re14_s83}}}{k_{\text{ic_re14_s20_s83}} + k_{\text{m_re14_s90_s83}} + [\text{AMP}(\text{matrix})]:[\text{H}+(\text{inner membrane space})]} \right) [\text{ATPsyn}]:[\text{H}+(\text{inner membrane space})]:[\text{AMP}(\text{matrix})] \right)
 \end{aligned}$$

$$\begin{aligned}
 \frac{d(\{NAM\}_{matrix}) \cdot V_{matrix}}{dt} &= +V_{matrix} \cdot (k_1^{[SIRT3]_{matrix}} \cdot [inhb(matrix)]) \\
 &- V_{matrix} \cdot (k_1^{[SIRT3]_{matrix}} \cdot \{NAM\}_{matrix}) \cdot [aSIRT3] \\
 &+ V_{matrix} \cdot \left(\frac{kcat_{re13_s85}_{[SIRT3]_{matrix}} \cdot [aSIRT3] \cdot \{NAD\}_{matrix} \cdot [SOD2]}{kcat_{re13_s22_s85}_{[SIRT3]_{matrix}} \cdot kmc_{re13_s4_s85}_{[SIRT3]_{matrix}} + [SOD2] \cdot \{NAD\}_{matrix}} + kmc_{re13_s4_s85}_{[SIRT3]_{matrix}} \cdot [SOD2] + kmc_{re13_s22_s85}_{[SIRT3]_{matrix}} \cdot \{NAD\}_{matrix}} \right) \\
 &+ \left(\frac{V_{matrix} \cdot kcat_{re24_s85}_{[SIRT3]_{matrix}} \cdot [aSIRT3] \cdot \{NAD\}_{matrix} \cdot [FOXO3]}{kcat_{re24_s85}_{[SIRT3]_{matrix}} \cdot kmc_{re24_s4_s85}_{[SIRT3]_{matrix}} + [FOXO3] \cdot \{NAD\}_{matrix}} + kmc_{re24_s4_s85}_{[SIRT3]_{matrix}} \cdot [FOXO3] + kmc_{re24_s85}_{[SIRT3]_{matrix}} \cdot \{NAD\}_{matrix}} \right) \\
 &+ V_{matrix} \cdot \left(\frac{kcat_{re86_s127_s5}_{[SIRT3]_{matrix}} \cdot [aSIRT3] \cdot \{NAD\}_{matrix} \cdot [IDH2]}{kcat_{re86_s127_s5}_{[SIRT3]_{matrix}} \cdot kmc_{re86_s4_s5}_{[SIRT3]_{matrix}} + [IDH2] \cdot \{NAD\}_{matrix}} + kmc_{re86_s4_s5}_{[SIRT3]_{matrix}} \cdot [IDH2] + kmc_{re86_s127_s5}_{[SIRT3]_{matrix}} \cdot \{NAD\}_{matrix}} \right) \\
 &- V_{matrix} \cdot (k_1^{[SIRT3]_{matrix}} \cdot \{NAM\}_{matrix}) \cdot [PRPP(matrix)] \\
 \\
 \frac{d(\{aSIRT3\}) \cdot V_{matrix}}{dt} &= -V_{matrix} \cdot (k_1^{[SIRT3]_{matrix}} \cdot [aSIRT3]) \\
 &+ V_{matrix} \cdot (k_1^{[SIRT3]_{matrix}} \cdot [inhb(matrix)]) \\
 &- V_{matrix} \cdot (k_1^{[SIRT3]_{matrix}} \cdot \{NAM\}_{matrix}) \cdot [aSIRT3] \\
 &+ V_{matrix} \cdot \left(\frac{kcat_{re1_s14}_{[SIRT3]_{matrix}} \cdot [SIRT3]}{kmc_{re1_s14}_{[SIRT3]_{matrix}} + [SIRT3]} \right) \\
 \\
 \frac{d(\{aAMPK\}) \cdot V_{cell}}{dt} &= +V_{cell} \cdot \left(\frac{kcat_{re20_s70}_{[AMPK]_{cell}} \cdot [aLKB1] \cdot [AMP(ce8)] \cdot [AMPK]}{kcat_{re20_s29_s70}_{[AMPK]_{cell}} \cdot kmc_{re20_s116_s70}_{[AMPK]_{cell}} + [AMPK] \cdot [AMP(ce8)] + kcat_{re20_s116_s70}_{[AMPK]_{cell}} \cdot [AMPK] + kmc_{re20_s29_s70}_{[AMPK]_{cell}} \cdot [AMP(ce8)]} \right) \\
 &- V_{cell} \cdot \left(\frac{V_{cell} \cdot k_{re21}_{[AMPK]_{cell}} \cdot [aAMPK] \cdot [ATP(ce8)]}{V_{cell}} \right) \\
 \\
 \frac{d(\{SIRT1\}) \cdot V_{cell}}{dt} &= +V_{cell} \cdot (k_1^{[SIRT1]_{cell}} \cdot [inhb(ce8)]) \\
 &- V_{cell} \cdot (k_1^{[SIRT1]_{cell}} \cdot \{NAM\}_{cell}) \cdot [SIRT1] \\
 \\
 \frac{d(\{aFOXO3\}) \cdot V_{cell}}{dt} &= -V_{cell} \cdot (k_1^{[FOXO3]_{cell}} \cdot [aFOXO3]) \\
 &+ V_{cell} \cdot \left(\frac{kcat_{re13_s85}_{[SIRT1]_{cell}} \cdot [SIRT1] \cdot \{NAD\}_{cell} \cdot [p_ac_FOXO3]}{kcat_{re13_s22_s85}_{[SIRT1]_{cell}} \cdot kmc_{re13_s4_s85}_{[SIRT1]_{cell}} + [p_ac_FOXO3] \cdot \{NAD\}_{cell}} + kmc_{re13_s4_s85}_{[SIRT1]_{cell}} \cdot [p_ac_FOXO3] + kmc_{re13_s22_s85}_{[SIRT1]_{cell}} \cdot \{NAD\}_{cell}} \right) \\
 \\
 \frac{d(\{PRPP(ce8)\}) \cdot V_{cell}}{dt} &= +V_{cell} \cdot \left(\frac{kcat_{re38_s104}_{[PRPP(ce8)]_{cell}} \cdot [NAMPT] \cdot [PRPP(ce8)] \cdot [NAM(ce8)]}{kcat_{re38_s104}_{[PRPP(ce8)]_{cell}} \cdot kmc_{re38_s101_s104}_{[PRPP(ce8)]_{cell}} + [NAMPT] \cdot [PRPP(ce8)] + kmc_{re38_s101_s104}_{[PRPP(ce8)]_{cell}} \cdot [NAM(ce8)] + kmc_{re38_s113_s104}_{[PRPP(ce8)]_{cell}} \cdot [PRPP(ce8)]} \right) \\
 &- V_{cell} \cdot \left(\frac{kcat_{re38_s104}_{[PRPP(ce8)]_{cell}} \cdot [NAMPT] \cdot [PRPP(ce8)] \cdot [NAM(ce8)]}{kcat_{re38_s104}_{[PRPP(ce8)]_{cell}} \cdot kmc_{re38_s101_s104}_{[PRPP(ce8)]_{cell}} + [NAMPT] \cdot [PRPP(ce8)] + kmc_{re38_s101_s104}_{[PRPP(ce8)]_{cell}} \cdot [NAM(ce8)] + kmc_{re38_s113_s104}_{[PRPP(ce8)]_{cell}} \cdot [PRPP(ce8)]} \right) \\
 \\
 \frac{d(\{NMN(ce8)\}) \cdot V_{cell}}{dt} &= +V_{cell} \cdot \left(\frac{kcat_{re38_s104}_{[NMNPT]_{cell}} \cdot [PRPP(ce8)] \cdot [NAM(ce8)]}{kcat_{re38_s104}_{[NMNPT]_{cell}} \cdot kmc_{re38_s101_s104}_{[NMNPT]_{cell}} + [NMNPT] \cdot [PRPP(ce8)] + kmc_{re38_s101_s104}_{[NMNPT]_{cell}} \cdot [NAM(ce8)] + kmc_{re38_s113_s104}_{[NMNPT]_{cell}} \cdot [PRPP(ce8)]} \right) \\
 &- V_{cell} \cdot \left(\frac{kcat_{re40_s105}_{[NMN(ce8)]_{cell}} \cdot [NMN(ce8)]}{kmc_{re40_s102_s105}_{[NMN(ce8)]_{cell}} + [NMN(ce8)]} \right) \\
 \\
 \frac{d(\{inhb(matrix)\}) \cdot V_{matrix}}{dt} &= -V_{matrix} \cdot (k_1^{[SIRT3]_{matrix}} \cdot [inhb(matrix)]) \\
 &+ V_{matrix} \cdot (k_1^{[SIRT3]_{matrix}} \cdot \{NAM\}_{matrix}) \cdot [aSIRT3] \\
 \\
 \frac{d(\{NAM(ce8)\}) \cdot V_{cell}}{dt} &= +V_{cell} \cdot (k_1^{[SIRT1]_{cell}} \cdot [inhb(ce8)]) \\
 &- V_{cell} \cdot (k_1^{[SIRT1]_{cell}} \cdot \{NAM\}_{cell}) \cdot [SIRT1] \\
 &+ V_{cell} \cdot \left(\frac{kcat_{re37_s88}_{[SIRT1]_{cell}} \cdot [SIRT1] \cdot \{NAD\}_{cell} \cdot [LKB1]}{kcat_{re37_s69_s88}_{[SIRT1]_{cell}} \cdot kmc_{re37_s114_s88}_{[SIRT1]_{cell}} + [LKB1] \cdot \{NAD\}_{cell}} + kmc_{re37_s114_s88}_{[SIRT1]_{cell}} \cdot [LKB1] + kmc_{re37_s69_s88}_{[SIRT1]_{cell}} \cdot \{NAD\}_{cell}} \right) \\
 &+ V_{cell} \cdot \left(\frac{kcat_{re13_s85}_{[SIRT1]_{cell}} \cdot [SIRT1] \cdot \{NAD\}_{cell} \cdot [p_ac_FOXO3]}{kcat_{re13_s22_s85}_{[SIRT1]_{cell}} \cdot kmc_{re13_s4_s85}_{[SIRT1]_{cell}} + [p_ac_FOXO3] \cdot \{NAD\}_{cell}} + kmc_{re13_s4_s85}_{[SIRT1]_{cell}} \cdot [p_ac_FOXO3] + kmc_{re13_s22_s85}_{[SIRT1]_{cell}} \cdot \{NAD\}_{cell}} \right) \\
 &+ V_{cell} \cdot \left(\frac{kcat_{re13_s85}_{[SIRT1]_{cell}} \cdot [SIRT1] \cdot \{NAD\}_{cell} \cdot [pac_PGC1a]}{kcat_{re13_s22_s85}_{[SIRT1]_{cell}} \cdot kmc_{re13_s4_s85}_{[SIRT1]_{cell}} + [pac_PGC1a] \cdot \{NAD\}_{cell}} + kmc_{re13_s4_s85}_{[SIRT1]_{cell}} \cdot [pac_PGC1a] + kmc_{re13_s22_s85}_{[SIRT1]_{cell}} \cdot \{NAD\}_{cell}} \right) \\
 &- V_{cell} \cdot \left(\frac{kcat_{re38_s104}_{[NAMPT]_{cell}} \cdot [PRPP(ce8)] \cdot [NAM(ce8)]}{kcat_{re38_s104}_{[NAMPT]_{cell}} \cdot kmc_{re38_s101_s104}_{[NAMPT]_{cell}} + [NAMPT] \cdot [PRPP(ce8)] + kmc_{re38_s101_s104}_{[NAMPT]_{cell}} \cdot [NAM(ce8)] + kmc_{re38_s113_s104}_{[NAMPT]_{cell}} \cdot [PRPP(ce8)]} \right) \\
 \\
 \frac{d(\{NAD(ce8)\}) \cdot V_{cell}}{dt} &= +V_{cell} \cdot (k_1^{[NADH]_{cell}} \cdot [NADH(ce8)]) \\
 &- V_{cell} \cdot (k_1^{[NAD]_{cell}} \cdot [NAD(ce8)]) \\
 &+ V_{cell} \cdot \left(\frac{kcat_{re54_s86}_{[NADH(ce8)]_{cell}} \cdot [NADH(ce8)]}{kmc_{re54_s123_s86}_{[NADH(ce8)]_{cell}} + [NADH(ce8)]} \right) \\
 &- V_{cell} \cdot \left(\frac{kcat_{re37_s88}_{[SIRT1]_{cell}} \cdot [SIRT1] \cdot \{NAD(ce8)\} \cdot [LKB1]}{kcat_{re37_s69_s88}_{[SIRT1]_{cell}} \cdot kmc_{re37_s114_s88}_{[SIRT1]_{cell}} + [LKB1] \cdot \{NAD(ce8)\}} + kmc_{re37_s114_s88}_{[SIRT1]_{cell}} \cdot [LKB1] + kmc_{re37_s69_s88}_{[SIRT1]_{cell}} \cdot \{NAD(ce8)\}} \right) \\
 &- V_{cell} \cdot \left(\frac{kcat_{re13_s85}_{[SIRT1]_{cell}} \cdot [SIRT1] \cdot \{NAD(ce8)\} \cdot [p_ac_FOXO3]}{kcat_{re13_s22_s85}_{[SIRT1]_{cell}} \cdot kmc_{re13_s4_s85}_{[SIRT1]_{cell}} + [p_ac_FOXO3] \cdot \{NAD(ce8)\}} + kmc_{re13_s4_s85}_{[SIRT1]_{cell}} \cdot [p_ac_FOXO3] + kmc_{re13_s22_s85}_{[SIRT1]_{cell}} \cdot \{NAD(ce8)\}} \right) \\
 &- V_{cell} \cdot \left(\frac{kcat_{re13_s85}_{[SIRT1]_{cell}} \cdot [SIRT1] \cdot \{NAD(ce8)\} \cdot [pac_PGC1a]}{kcat_{re13_s22_s85}_{[SIRT1]_{cell}} \cdot kmc_{re13_s4_s85}_{[SIRT1]_{cell}} + [pac_PGC1a] \cdot \{NAD(ce8)\}} + kmc_{re13_s4_s85}_{[SIRT1]_{cell}} \cdot [pac_PGC1a] + kmc_{re13_s22_s85}_{[SIRT1]_{cell}} \cdot \{NAD(ce8)\}} \right) \\
 &+ V_{cell} \cdot \left(\frac{kcat_{re40_s105}_{[NMN(ce8)]_{cell}} \cdot [NMN(ce8)]}{kmc_{re40_s102_s105}_{[NMN(ce8)]_{cell}} + [NMN(ce8)]} \right) \\
 \end{aligned}$$

$$\begin{aligned} \frac{d([e]) \cdot V_{matrix}}{dt} &= -V_{matrix} \left(\frac{[ETC] \cdot k_{cat_re9_s21} \cdot [e]}{k_{m_re9_s17_s21} + [e]} + \frac{[O2]}{[H^+ (matrix)]} \right) \\ &\quad - V_{matrix} \cdot (k_1^{(cyto)}} \cdot [e] \cdot [O2]) \\ &\quad + V_{matrix} \cdot [ETC] \cdot \frac{k_{cat_re7_s21} \cdot [NADH(matrix)]}{k_{m_re7_s16_s21} + [NADH(matrix)]} \\ \frac{d([IDH2]) \cdot V_{matrix}}{dt} &= +V_{matrix} \cdot (k_1^{(cyto)}} \cdot [aIDH2]) \\ &\quad - V_{matrix} \cdot \left(\frac{k_{cat_re86_s5} \cdot [aSIRT3] \cdot [NAD(matrix)] \cdot [IDH2]}{k_{m_re86_s127_s5} + k_{m_re86_s4_s5} + [IDH2] \cdot [NAD(matrix)] + k_{m_re86_s4_s5} \cdot [IDH2] + k_{m_re86_s127_s5} \cdot [NAD(matrix)]} \right) \\ \frac{d([aPGC1a]) \cdot V_{cell}}{dt} &= -V_{cell} \cdot (k_1^{(cyto)}} \cdot [aPGC1a]) \\ &\quad + V_{cell} \cdot \left(\frac{k_{cat_re13_s85} \cdot [SIRT1] \cdot [NAD(cell)] \cdot [pac_PGC1a]}{k_{m_re13_s22_s85} + k_{m_re13_s4_s85} + [pac_PGC1a] \cdot [NAD(cell)] + k_{m_re13_s4_s85} \cdot [pac_PGC1a] + k_{m_re13_s22_s85} \cdot [NAD(cell)]} \right) \\ \frac{d([pac_PGC1a]) \cdot V_{cell}}{dt} &= +V_{cell} \cdot (k_1^{(cyto)}} \cdot [aPGC1a]) \\ &\quad - V_{cell} \cdot (k_1^{(cyto)}} \cdot [pac_PGC1a]) \\ &\quad + V_{cell} \cdot \left([aAMPK] \cdot \frac{k_{cat_re69_s86} \cdot [pac_PGC1a]}{k_{m_re69_s133_s86} + [pac_PGC1a]} \right) \\ &\quad - V_{cell} \cdot \left(\frac{k_{cat_re13_s85} \cdot [SIRT1] \cdot [NAD(cell)] \cdot [pac_PGC1a]}{k_{m_re13_s22_s85} + k_{m_re13_s4_s85} + [pac_PGC1a] \cdot [NAD(cell)] + k_{m_re13_s4_s85} \cdot [pac_PGC1a] + k_{m_re13_s22_s85} \cdot [NAD(cell)]} \right) \\ \frac{d([ac_PGC1a]) \cdot V_{cell}}{dt} &= +V_{cell} \cdot (k_1^{(cyto)}} \cdot [pac_PGC1a]) \\ &\quad - V_{cell} \cdot \left([aAMPK] \cdot \frac{k_{cat_re69_s86} \cdot [pac_PGC1a]}{k_{m_re69_s133_s86} + [pac_PGC1a]} \right) \\ \frac{d([p_ac_FOXO3]) \cdot V_{cell}}{dt} &= +V_{cell} \cdot (k_1^{(cyto)}} \cdot [aFOXO3]) \\ &\quad + V_{cell} \cdot \left([aAMPK] \cdot \frac{k_{cat_re36_s86} \cdot [ac_FOXO3(cell)]}{k_{m_re36_s34_s86} + [ac_FOXO3(cell)]} \right) \\ &\quad - V_{cell} \cdot \left(\frac{k_{cat_re13_s85} \cdot [SIRT1] \cdot [NAD(cell)] \cdot [p_ac_FOXO3]}{k_{m_re13_s22_s85} + k_{m_re13_s4_s85} + [p_ac_FOXO3] \cdot [NAD(cell)] + k_{m_re13_s4_s85} \cdot [p_ac_FOXO3] + k_{m_re13_s22_s85} \cdot [NAD(cell)]} \right) \\ &\quad - V_{cell} \cdot (k_1^{(cyto)}} \cdot [p_ac_FOXO3]) \\ \frac{d([ac_FOXO3(cell)]) \cdot V_{cell}}{dt} &= -V_{cell} \cdot (k_1^{(cyto)}} \cdot [ac_FOXO3(cell)]) \\ &\quad + V_{cell} \cdot \left(\frac{V_{matrix} \cdot k_{cat_re24_s85} \cdot [aSIRT3] \cdot [NAD(matrix)] \cdot [FOXO3]}{k_{m_re24_s81_s85} + k_{m_re24_s4_s85} + [FOXO3] \cdot [NAD(matrix)] + k_{m_re24_s4_s85} \cdot [FOXO3] + k_{m_re24_s81_s85} \cdot [NAD(matrix)]} \right) \\ &\quad - V_{cell} \cdot \left([aAMPK] \cdot \frac{k_{cat_re36_s86} \cdot [ac_FOXO3(cell)]}{k_{m_re36_s34_s86} + [ac_FOXO3(cell)]} \right) \\ &\quad + V_{cell} \cdot (k_1^{(cyto)}} \cdot [p_ac_FOXO3]) \\ \frac{d([FOXO3]) \cdot V_{matrix}}{dt} &= +V_{cell} \cdot (k_1^{(cyto)}} \cdot [ac_FOXO3(cell)]) \\ &\quad - V_{matrix} \cdot \left(\frac{V_{matrix} \cdot k_{cat_re24_s85} \cdot [aSIRT3] \cdot [NAD(matrix)] \cdot [FOXO3]}{k_{m_re24_s81_s85} + k_{m_re24_s4_s85} + [FOXO3] \cdot [NAD(matrix)] + k_{m_re24_s4_s85} \cdot [FOXO3] + k_{m_re24_s81_s85} \cdot [NAD(matrix)]} \right) \\ \frac{d([aIDH2]) \cdot V_{matrix}}{dt} &= -V_{matrix} \cdot (k_1^{(cyto)}} \cdot [aIDH2]) \\ &\quad + V_{matrix} \cdot \left(\frac{k_{cat_re86_s5} \cdot [aSIRT3] \cdot [NAD(matrix)] \cdot [IDH2]}{k_{m_re86_s127_s5} + k_{m_re86_s4_s5} + [IDH2] \cdot [NAD(matrix)] + k_{m_re86_s4_s5} \cdot [IDH2] + k_{m_re86_s127_s5} \cdot [NAD(matrix)]} \right) \\ \text{"Proton Grad"} &= \frac{[H^+ (matrix)]}{[H^+ (matrix)]} \\ \text{*ATP/AMP (matrix)*} &= \frac{ATP(matrix) \cdot ParticleNumber}{AMP(matrix) \cdot ParticleNumber} \\ \text{*NAD/NADH (cyto)*} &= \frac{[NAD(cell)]}{[NADH(cell)]} \\ \text{*NAD/NADH (matrix)*} &= \frac{[NAD(matrix)]}{[NADH(matrix)]} \end{aligned}$$

Initial State

Initial Compartment Sizes

default	1 l	
matrix	6.83e-19 l	
inner membrane space		2.28e-19 l
cell	1e-13 l	

Initial Species Values

ETC	4.408 $\mu\text{mol}/(\text{l})$
ATPsyn	26.9466 $\mu\text{mol}/(\text{l})$
SOD2	53.759 $\mu\text{mol}/(\text{l})$
NADH{matrix}	12 $\mu\text{mol}/(\text{l})$
aSOD2	17.9197 $\mu\text{mol}/(\text{l})$
Cat	15.1617 $\mu\text{mol}/(\text{l})$
AMP{matrix}	0.0014 $\mu\text{mol}/(\text{l})$
ATP{matrix}	1390 $\mu\text{mol}/(\text{l})$
GSSG	0.041 $\mu\text{mol}/(\text{l})$
GSH	1.2 $\mu\text{mol}/(\text{l})$
NADP+	19.6 $\mu\text{mol}/(\text{l})$
NADPH	51 $\mu\text{mol}/(\text{l})$
GPx	17.4155 $\mu\text{mol}/(\text{l})$
GR	0.5972 $\mu\text{mol}/(\text{l})$
LKB1	0.1789 $\mu\text{mol}/(\text{l})$
aLKB1	0.0596 $\mu\text{mol}/(\text{l})$
AMPK	0.0533 $\mu\text{mol}/(\text{l})$
PRPP{matrix}	6.67 $\mu\text{mol}/(\text{l})$
PPi{matrix}	0 $\mu\text{mol}/(\text{l})$
NMN{matrix}	0.0589 $\mu\text{mol}/(\text{l})$
NAD{matrix}	50 $\mu\text{mol}/(\text{l})$
SIRT3	0.0075 $\mu\text{mol}/(\text{l})$
NAM{matrix}	0.4809 $\mu\text{mol}/(\text{l})$
aSIRT3	0.0013 $\mu\text{mol}/(\text{l})$
aAMPK	0.0178 $\mu\text{mol}/(\text{l})$
SIRT1	0.0036 $\mu\text{mol}/(\text{l})$
aFOXO3	0.00099 $\mu\text{mol}/(\text{l})$
PPi{cell}	0 $\mu\text{mol}/(\text{l})$
PRPP{cell}	4.9 $\mu\text{mol}/(\text{l})$
NMN{cell}	0.0589 $\mu\text{mol}/(\text{l})$
NAMPT	0.4809 $\mu\text{mol}/(\text{l})$
NMNAT	0.0049 $\mu\text{mol}/(\text{l})$
NMNAT3	0.0664 $\mu\text{mol}/(\text{l})$
inhib{matrix}	0.0012 $\mu\text{mol}/(\text{l})$
NAM{cell}	0.4809 $\mu\text{mol}/(\text{l})$
NAD{cell}	85 $\mu\text{mol}/(\text{l})$
ATP{cell}	1390 $\mu\text{mol}/(\text{l})$
AMP{cell}	0.0014 $\mu\text{mol}/(\text{l})$
O2'	0 $\mu\text{mol}/(\text{l})$
H2O2	10.5 $\mu\text{mol}/(\text{l})$
H+{matrix}	0.0048 $\mu\text{mol}/(\text{l})$
H+{"inner membrane space"}	0.1 $\mu\text{mol}/(\text{l})$
H2O	0 $\mu\text{mol}/(\text{l})$
O2	32 $\mu\text{mol}/(\text{l})$
NADH{cell}	1.17 $\mu\text{mol}/(\text{l})$
inhib{cell}	0.0012 $\mu\text{mol}/(\text{l})$

e	0 $\mu\text{mol}/(\text{l})$
IDH2	8.7951 $\mu\text{mol}/(\text{l})$
aPGC1a	1.1e-05 $\mu\text{mol}/(\text{l})$
pac_PGC1a	7.7e-05 $\mu\text{mol}/(\text{l})$
ac_PGC1a	1.65e-05 $\mu\text{mol}/(\text{l})$
p_ac_FOXO3	0.003 $\mu\text{mol}/(\text{l})$
ac_FOXO3{cell}	0.0118 $\mu\text{mol}/(\text{l})$
FOXO3	0.0039 $\mu\text{mol}/(\text{l})$
aIDH2	2.9317 $\mu\text{mol}/(\text{l})$
metabolic	1 $\mu\text{mol}/(\text{l})$
UCP5	1 $\mu\text{mol}/(\text{l})$
Initial Global Quantities	
Proton Grad	20.8333 dimensionless
ATP/AMP {matrix}	992857 dimensionless
NAD/NADH {cyto}	72.6496 dimensionless
NAD/NADH {matrix}	4.16667 dimensionless
Kinetic Parameters	
SIRT3 deact	
k1	0.0607443 1/min
SIRT3 disinhib	
k1	0.031598 1/min
NAD rdxn {matrix}	
kcat_re40_s105	9.184 1/min
kmc_re40_s102_s105	1.5072e-06 $\mu\text{mol}/\text{l}$
AMP transport	
kf_re46	1e-05 1/min
ATP consump {mtx}	
k1	0.125164 1/min
SOD2 deact	
k1	0.00271808 1/min
AMPK deact	
kf_re21	0.0183318 $\text{l}/(\mu\text{mol}*\text{min})$
FOXO3 dephos	
k1	1.24677e-05 1/min
NAM->NMN{mtx}	
k1	111.534 $\text{l}/(\mu\text{mol}*\text{min})$
LKB1 deact	
k1	0.0338412 1/min
FOXO3 to matrix	
kf_re35	0.0278129 1/min
SIRT3 inhib	
k1	1e-05 $\text{l}/(\mu\text{mol}*\text{min})$
SIRT1 disinhib	
k1	1.09474 1/min
NADH oxdtn {cyto}	
k1	0.13173 1/min
ATP export	
kf_re47	17.5096 1/min
ATP hydrolysis	
k1	0.23558 1/min
SIRT1 inhib	
k1	0.0103606 $\text{l}/(\mu\text{mol}*\text{min})$
NAD rdxn {cyto}	
k1	0.00513173 1/min
PGC1a acyl	

k1	0.00109024 1/min
PGC1a	
k1	0.0386717 1/min
FOXO3a deact	
k1	0.0195509 1/min
H2O2 decomp (Cat)	
kcat_re10_s3	0.001248 1/min
kmc_re10_s18_s3	7.36 $\mu\text{mol/l}$
SIRT3 act	
kcat_re1_s14	0.0257019 1/min
kmc_re1_s5_s14	0.0153836 $\mu\text{mol/l}$
e capture	
kcat_re9_s21	1.264e-05 1/min
kmc_re9_s17_s21	0.0353064 $\mu\text{mol/l}$
kmc_re9_s11_s21	0.0143592 $\mu\text{mol/l}$
kmc_re9_s6_s21	0.0242807 $\mu\text{mol/l}$
O2 rad formation	
k1	1e-05 l/($\mu\text{mol}^*\text{min}$)
NADH ox (ETC)	
kcat_re7_s21	2.94443 1/min
kmc_re7_s16_s21	0.458844 $\mu\text{mol/l}$
Peroxide formation (SOD2)	
kcat_re4_s24	27.456 1/min
kmc_re4_s14_s24	0.007 $\mu\text{mol/l}$
kmc_re4_s6_s24	0.004992 $\mu\text{mol/l}$
kic_re4_s14_s24	0.01 $\mu\text{mol/l}$
NMN->NAD{matrix}	
kcat_re27_s51	112.176 1/min
kmc_re27_s47_s51	87.1298 $\mu\text{mol/l}$
H2O2 decomp (Gpx)	
kcat_re11_s63	30.4704 1/min
kmc_re11_s18_s63	5 $\mu\text{mol/l}$
kmc_re11_s60_s63	2.88 $\mu\text{mol/l}$
kic_re11_s18_s63	0.00408 $\mu\text{mol/l}$
GSSG rdxn	
kcat_re18_s64	304.261 1/min
kmc_re18_s59_s64	37.516 $\mu\text{mol/l}$
kmc_re18_s62_s64	7.6109 $\mu\text{mol/l}$
kic_re18_s59_s64	0.0117007 $\mu\text{mol/l}$
AMPK activation	
kcat_re20_s70	2.16999 1/min
kmc_re20_s29_s70	14.7446 $\mu\text{mol/l}$
kmc_re20_s116_s70	18.14 $\mu\text{mol/l}$
kic_re20_s29_s70	7.40837 $\mu\text{mol/l}$
ATP syn	
kcat_re14_s83	1e-05 1/min
kmc_re14_s20_s83	0.226778 $\mu\text{mol/l}$
kmc_re14_s90_s83	0.0743971 $\mu\text{mol/l}$
kic_re14_s20_s83	0.110651 $\mu\text{mol/l}$
SOD2 act	
kcat_re13_s85	1.44757 1/min
kmc_re13_s22_s85	1e-05 $\mu\text{mol/l}$
kmc_re13_s4_s85	1e-05 $\mu\text{mol/l}$
kic_re13_s22_s85	0.0787856 $\mu\text{mol/l}$
FOXO3a exp	

kcat_re24_s85	3.24781 1/min
kmc_re24_s81_s85	1e-05 $\mu\text{mol/l}$
kmc_re24_s4_s85	1e-05 $\mu\text{mol/l}$
kic_re24_s81_s85	132.145 $\mu\text{mol/l}$
NADH ox	
kcat_re54_s86	1213.99 1/min
kmc_re54_s123_s86	7.18526 $\mu\text{mol/l}$
PGC1a phos	
kcat_re69_s86	5.43493 1/min
kmc_re69_s133_s86	0.00896693 $\mu\text{mol/l}$
FOXO3a phos	
kcat_re36_s86	1.07218 1/min
kmc_re36_s34_s86	0.0239716 $\mu\text{mol/l}$
LKB1 act	
kcat_re37_s88	0.269103 1/min
kmc_re37_s69_s88	31.4614 $\mu\text{mol/l}$
kmc_re37_s114_s88	205.788 $\mu\text{mol/l}$
kic_re37_s69_s88	5.27956 $\mu\text{mol/l}$
FOXO3 act	
kcat_re13_s85	159.577 1/min
kic_re13_s22_s85	260.251 $\mu\text{mol/l}$
kmc_re13_s22_s85	117.909 $\mu\text{mol/l}$
kmc_re13_s4_s85	1.95425 $\mu\text{mol/l}$
PGC1 deacyl	
kcat_re13_s85	0.0220595 1/min
kic_re13_s22_s85	53.1197 $\mu\text{mol/l}$
kmc_re13_s22_s85	183.867 $\mu\text{mol/l}$
kmc_re13_s4_s85	2.67021 $\mu\text{mol/l}$
NAM->NMN{cell}	
kcat_re38_s104	21.1889 1/min
kmc_re38_s113_s104	41.2056 $\mu\text{mol/l}$
kmc_re38_s101_s104	0.860579 $\mu\text{mol/l}$
kic_re38_s113_s104	0.00753388 $\mu\text{mol/l}$
NMN->NAD{cell}	
kcat_re40_s105	0.655759 1/min
kmc_re40_s102_s105	47.1165 $\mu\text{mol/l}$
NADP rdxn	
kcat_re73_s127	1e-05 1/min
kmc_re73_s61_s127	12.0712 $\mu\text{mol/l}$
kmc_re73_s6_s127	99.8827 $\mu\text{mol/l}$
kic_re73_s61_s127	0.01616 $\mu\text{mol/l}$
IDH2 deact	
k1	0.0444651 1/min
IDH2 act	
kcat_re86_s5	50.985 1/min
kmc_re86_s127_s5	1e-05 $\mu\text{mol/l}$
kmc_re86_s4_s5	4.62915 $\mu\text{mol/l}$
kic_re86_s127_s5	1e-05 $\mu\text{mol/l}$
H+ leak	
k1	0.00026904 1/min

Initial State

Kinetic Parameters

SIRT3 deact	nan $\mu\text{mol}/(\text{l}^*\text{min})$
k1	1.8 1/min
SIRT3 disinhib	nan $\mu\text{mol}/(\text{l}^*\text{min})$
k1	0.0197 1/min
NAD rdxn {matrix}	nan $\mu\text{mol}/(\text{l}^*\text{min})$
kcat_re40_s105	1.04781 1/min
kmc_re40_s102_s105	0.021257 $\mu\text{mol}/\text{l}$
AMP transport	nan $\mu\text{mol}/(\text{min})$
kf_re46	0.24 1/min
ATP consump {mtx}	nan $\mu\text{mol}/(\text{l}^*\text{min})$
k1	0.204 1/min
SOD2 deact	nan $\mu\text{mol}/(\text{l}^*\text{min})$
k1	0.03 1/min
AMPK deact	nan $\mu\text{mol}/(\text{l}^*\text{min})$
kf_re21	0.039 $\text{l}/(\mu\text{mol}^*\text{min})$
FOXO3 dephos	nan $\mu\text{mol}/(\text{l}^*\text{min})$
k1	0.0001 1/min
NAM->NMN{mtx}	nan $\mu\text{mol}/(\text{l}^*\text{min})$
k1	32 $\text{l}/(\mu\text{mol}^*\text{min})$
LKB1 deact	nan $\mu\text{mol}/(\text{l}^*\text{min})$
k1	0.03 1/min
FOXO3 to matrix	nan $\mu\text{mol}/(\text{min})$
kf_re35	0.24 1/min
SIRT3 inhib	nan $\mu\text{mol}/(\text{l}^*\text{min})$
k1	0.197 $\text{l}/(\mu\text{mol}^*\text{min})$
SIRT1 disinhib	nan $\mu\text{mol}/(\text{l}^*\text{min})$
k1	1.79 1/min
NADH oxdtm {cyto}	nan $\mu\text{mol}/(\text{l}^*\text{min})$
k1	0.05 1/min
ATP export	nan $\mu\text{mol}/(\text{min})$
kf_re47	9.6 1/min
ATP hydrolysis	nan $\mu\text{mol}/(\text{l}^*\text{min})$
k1	0.204 1/min
SIRT1 inhib	nan $\mu\text{mol}/(\text{l}^*\text{min})$
k1	0.01 $\text{l}/(\mu\text{mol}^*\text{min})$
NAD rdxn {cyto}	nan $\mu\text{mol}/(\text{l}^*\text{min})$
k1	0.01 1/min
PGC1a acyl	nan $\mu\text{mol}/(\text{l}^*\text{min})$
k1	0.03 1/min
PGC1a	nan $\mu\text{mol}/(\text{l}^*\text{min})$
k1	0.03 1/min
FOXO3a deact	nan $\mu\text{mol}/(\text{l}^*\text{min})$
k1	0.03 1/min
H2O2 decomp (Cat)	nan $\mu\text{mol}/(\text{l}^*\text{min})$
kcat_re10_s3	0.0012 1/min
kmc_re10_s18_s3	20 $\mu\text{mol}/\text{l}$
SIRT3 act	nan $\mu\text{mol}/(\text{l}^*\text{min})$
kcat_re1_s14	0.03 1/min
kmc_re1_s5_s14	0.2 $\mu\text{mol}/\text{l}$
e capture	nan $\mu\text{mol}/(\text{l}^*\text{min})$
kcat_re9_s21	10 1/min

kmc_re9_s17_s21	0.01 $\mu\text{mol/l}$
kmc_re9_s11_s21	0.01 $\mu\text{mol/l}$
kmc_re9_s6_s21	0.01 $\mu\text{mol/l}$
O2 rad formation	nan $\mu\text{mol}/(\text{l}^*\text{min})$
k1	0.57 $\text{l}/(\mu\text{mol}^*\text{min})$
NADH ox (ETC)	nan $\mu\text{mol}/(\text{min})$
kcat_re7_s21	1 $1/\text{min}$
kmc_re7_s16_s21	0.01 $\mu\text{mol/l}$
Peroxide formation (SOD2)	nan $\mu\text{mol}/(\text{l}^*\text{min})$
kcat_re4_s24	24 $1/\text{min}$
kmc_re4_s14_s24	0.005 $\mu\text{mol/l}$
kmc_re4_s6_s24	0.005 $\mu\text{mol/l}$
kic_re4_s14_s24	0.01 $\mu\text{mol/l}$
NMN->NAD{matrix}	nan $\mu\text{mol}/(\text{l}^*\text{min})$
kcat_re27_s51	150 $1/\text{min}$
kmc_re27_s47_s51	66.2 $\mu\text{mol/l}$
H2O2 decomp (Gpx)	nan $\mu\text{mol}/(\text{l}^*\text{min})$
kcat_re11_s63	31.74 $1/\text{min}$
kmc_re11_s18_s63	5 $\mu\text{mol/l}$
kmc_re11_s60_s63	2 $\mu\text{mol/l}$
kic_re11_s18_s63	0.01 $\mu\text{mol/l}$
GSSG rdxn	nan $\mu\text{mol}/(\text{l}^*\text{min})$
kcat_re18_s64	144 $1/\text{min}$
kmc_re18_s59_s64	56.7 $\mu\text{mol/l}$
kmc_re18_s62_s64	7.9 $\mu\text{mol/l}$
kic_re18_s59_s64	0.01 $\mu\text{mol/l}$
AMPK activation	nan $\mu\text{mol}/(\text{l}^*\text{min})$
kcat_re20_s70	10 $1/\text{min}$
kmc_re20_s29_s70	67.2 $\mu\text{mol/l}$
kmc_re20_s116_s70	48 $\mu\text{mol/l}$
kic_re20_s29_s70	67.2 $\mu\text{mol/l}$
ATP syn	nan $\mu\text{mol}/(\text{min})$
kcat_re14_s83	0.5 $1/\text{min}$
kmc_re14_s20_s83	0.1 $\mu\text{mol/l}$
kmc_re14_s90_s83	0.1 $\mu\text{mol/l}$
kic_re14_s20_s83	0.01 $\mu\text{mol/l}$
SOD2 act	nan $\mu\text{mol}/(\text{l}^*\text{min})$
kcat_re13_s85	0.197 $1/\text{min}$
kmc_re13_s22_s85	25.5 $\mu\text{mol/l}$
kmc_re13_s4_s85	140 $\mu\text{mol/l}$
kic_re13_s22_s85	29.4 $\mu\text{mol/l}$
FOXO3a exp	nan $\mu\text{mol}/(\text{min})$
kcat_re24_s85	0.197 $1/\text{min}$
kmc_re24_s81_s85	25.5 $\mu\text{mol/l}$
kmc_re24_s4_s85	673.3 $\mu\text{mol/l}$
kic_re24_s81_s85	29.4 $\mu\text{mol/l}$
NADH ox	nan $\mu\text{mol}/(\text{l}^*\text{min})$
kcat_re54_s86	270 $1/\text{min}$
kmc_re54_s123_s86	8 $\mu\text{mol/l}$
PGC1a phos	nan $\mu\text{mol}/(\text{l}^*\text{min})$
kcat_re69_s86	3.42 $1/\text{min}$
kmc_re69_s133_s86	0.0093 $\mu\text{mol/l}$
FOXO3a phos	nan $\mu\text{mol}/(\text{l}^*\text{min})$
kcat_re36_s86	0.72 $1/\text{min}$
kmc_re36_s34_s86	0.26 $\mu\text{mol/l}$

LKB1 act	nan $\mu\text{mol}/(\text{l}*\text{min})$
kcat_re37_s88	14.4 1/min
kmc_re37_s69_s88	25.5 $\mu\text{mol}/\text{l}$
kmc_re37_s114_s88	82.6 $\mu\text{mol}/\text{l}$
kic_re37_s69_s88	60.5 $\mu\text{mol}/\text{l}$
FOXO3 act	nan $\mu\text{mol}/(\text{l}*\text{min})$
kcat_re13_s85	14.4 1/min
kic_re13_s22_s85	60.5 $\mu\text{mol}/\text{l}$
kmc_re13_s22_s85	82.6 $\mu\text{mol}/\text{l}$
kmc_re13_s4_s85	25.5 $\mu\text{mol}/\text{l}$
PGC1 deacyl	nan $\mu\text{mol}/(\text{l}*\text{min})$
kcat_re13_s85	14.4 1/min
kic_re13_s22_s85	60.5 $\mu\text{mol}/\text{l}$
kmc_re13_s22_s85	82.6 $\mu\text{mol}/\text{l}$
kmc_re13_s4_s85	25.5 $\mu\text{mol}/\text{l}$
NAM->NMN{cell}	nan $\mu\text{mol}/(\text{l}*\text{min})$
kcat_re38_s104	32 1/min
kmc_re38_s113_s104	22.9 $\mu\text{mol}/\text{l}$
kmc_re38_s101_s104	2.67 $\mu\text{mol}/\text{l}$
kic_re38_s113_s104	0.05 $\mu\text{mol}/\text{l}$
NMN->NAD{cell}	nan $\mu\text{mol}/(\text{l}*\text{min})$
kcat_re40_s105	150 1/min
kmc_re40_s102_s105	66.2 $\mu\text{mol}/\text{l}$
NADP rdxn	nan $\mu\text{mol}/(\text{l}*\text{min})$
kcat_re73_s127	14400 1/min
kmc_re73_s61_s127	7.9 $\mu\text{mol}/\text{l}$
kmc_re73_s6_s127	56.7 $\mu\text{mol}/\text{l}$
kic_re73_s61_s127	0.01 $\mu\text{mol}/\text{l}$
IDH2 deact	nan $\mu\text{mol}/(\text{l}*\text{min})$
k1	0.03 1/min
IDH2 act	nan $\mu\text{mol}/(\text{l}*\text{min})$
kcat_re86_s5	14.4 1/min
kmc_re86_s127_s5	82.6 $\mu\text{mol}/\text{l}$
kmc_re86_s4_s5	25.5 $\mu\text{mol}/\text{l}$
kic_re86_s127_s5	60.5 $\mu\text{mol}/\text{l}$
H+ leak	nan $\mu\text{mol}/(\text{l}*\text{min})$
k1	1e-05 1/min